This is a repository copy of *Seismic-driven geocellular modeling of fluvial meander-belt reservoirs using a rule-based method*.

White Rose Research Online URL for this paper:
http://eprints.whiterose.ac.uk/129207/

Version: Accepted Version

Article:

Seismic-driven geocellular modeling of fluvial meander-belt reservoirs using a rule-based method

Luca Colombera[1,*], Na Yan[1], Tom McCormick-Cox[2], Nigel P. Mountney[1]

1) Fluvial & Eolian Research Group, School of Earth & Environment, University of Leeds, LS2 9JT, Leeds, UK
2) Shell B.V., Rijswijk, The Netherlands

*) corresponding author: l.colombera@leeds.ac.uk

Abstract

A novel workflow is presented for building static models of fluvial reservoirs composed of large point-bar architectural elements, based on the application of a specialized forward stratigraphic model, named 'Point-Bar Sedimentary Architecture Numerical Deduction' (PB-SAND).

The approach uses interpreted horizontal slices from 3D seismic datasets to reconstruct the planform evolution of meander loops, on which basis the geometry of point-bar deposits and associated accretion units can be simulated deterministically. The resulting meander-belt geometry is then populated with different types of facies, through a rule-based algorithm that generates facies architectures that reflect geologic understanding, enabling users to establish linkages between styles of meander evolution (e.g., meander growth via expansion, translation, rotation) and facies distributions. Input parameters define the proportions, geometries and distributions of types of point-bar deposits, as captured from subsurface data and/or from geologic analogs. Multiple stochastic realizations of facies architecture can be generated.

To demonstrate the application of this modeling approach, the workflow has been applied to a meander-belt reservoir where large point-bar and channel-fill elements are imaged in seismic. A detailed example is used to illustrate workflows that can be used to build high-resolution sector models in pre-drill contexts, suitable for guiding development plans. An additional example is used to show how to achieve well match for densely drilled sectors, by means of a hybrid approach that combines the new algorithm with traditional geostatistical techniques.

It is shown how the workflow allows consideration of point-bar growth styles, as inferred from seismic data, on distribution and geometry of heterogeneities, and how this facilitates the reproduction of geologic features that are important controls on the static connectivity of point-bar reservoirs (e.g., distribution and characteristics of bar-front mud drapes, and of mud-prone packages arising from progressive meander-bend tightening or from downstream fining of deposits beyond the apex of a meander bend). A comparison with traditional variogram-based methods is undertaken to compare metrics that describe intra-point-bar static connectivity and that represent proxies for the degree of compartmentalization of upper-bar sands by mud drapes.

Keywords: point bar; mud drape; meandering channel; sedimentary architecture; connectivity; reservoir model; facies model; stochastic model.

1. Introduction

Many hydrocarbon reservoirs are hosted in fluvial meander-belt successions, in which point-bar sands constitute the main reservoir units (e.g., Cornish 1984; Sonnenberg et al. 1990; Werren et al. 1990; Chapin & Meyer 1991; de Rooij et al. 2002; Carter 2003; Edie & Andrichuk 2005; Wu et al. 2008). Since the advent of three-dimensional (3D) seismic acquisitions, identification of individual point bars and channel fills that form the preserved product of large meandering channel belts has commonly been possible, and the recognition of such forms is important for enhanced subsurface characterization, based on interpretation of time or stratal slices (cf. Posamentier 2001; Miall 2002; Ethridge & Schumm 2007; Maynard et al. 2010; Reijenstein et al. 2011). Although only the external geometry of preserved point-bar or abandoned-channel-fill elements can be observed from seismic datasets in many cases (Feng 2000; Darmadi et al. 2007; El-Mowafy & Marfurt 2016; Gorain & Shalivahan 2018), in others the planform expression of the internal accretion geometry of point-bar deposits can be resolved (Maynard & Murray 2003; Fachmi & Wood 2005; Hubbard et al. 2011; Alqahtani et al. 2015). Given that types of meander evolution determine architectural styles that differ with respect to internal geometries and distribution of lithologies, 3D seismic data provide insight that can be used for qualitative predictions of lithologic heterogeneity (cf. Labrecque et al. 2011; Fustic et al. 2012). However, inclusion of this type of understanding into geocellular models is limited by the constraints imposed by geomodeling tools.

Traditional object- and pixel-based reservoir-modeling methods are commonly constrained using well, seismic and analog data (e.g., models fitted to experimental indicator variograms, sandbody geometries measured in outcrop analogs, training images; Deutsch & Journel 1998; Strebelle 2002; Colombera et al. 2012a, b). These models are conditioned on hard and soft data, typically consisting of well observations and seismic attributes, respectively (i.e., as descriptions of 'facies' occurrence and probability; Pyrcz & Deutsch 2014, and references therein). Direct integration of information on fluvial channel-belt accretion geometries as seen in seismic data is currently not achieved using tools that are commonly employed for stochastic reservoir modeling. Furthermore, common geostatistical techniques are difficult to apply in situations characterized by non-stationarity of the properties being modeled, in relation for example to trends in the distribution of lithologies in a point-bar element, which might be expressed as fining-upward, fining-outward through bend expansion, or fining downstream toward the bar-tail region (cf. Bluck 1971; Nanson & Page 1983; Wood 1989; van de Lageweg et al. 2014). These limitations are particularly important when considering the wide variability in styles of point-bar facies architectures and its impact on the static connectivity of sands (cf. Willis & Tang 2010). Nonetheless, in recent years, so-called rule-based modeling algorithms have been shown to represent a category of reservoir-modeling methods that holds promise as a way to reproduce complex geologic features and trends, thanks to each tool being specially designed for a specific geologic setting (Pyrcz et al. 2015, and references therein).

In this study we propose and illustrate the application of a workflow that applies the Point Bar Sedimentary Architecture Numerical Deduction (PB-SAND), a mixed deterministic-stochastic, rule-based algorithm for geometric modeling of point-bar facies architectures (Yan et al. 2017). The aim of the work is to demonstrate how such approach to modeling fluvial meander-belt reservoirs can

overcome the inability to use planforms from seismic datasets and to include geologic concepts in the generation of geocellular models.

By presenting outcomes from a selected case-study application of PB-SAND to reservoir modeling, this study has the following specific research objectives:

- To show workflows that permit integration of data from geologic analogs, wells and 3D seismic, for generating multiple realizations of the facies architecture of point-bar hydrocarbon reservoirs;
- To demonstrate how PB-SAND can be applied, in slightly different ways, in different situations of subsurface modeling (pre- and post-drill), each with different objectives (well design, secondary and enhanced oil recovery);
- To compare the method output quantitatively against its counterpart from a commonly employed modeling technique, by means of comparison of static-connectivity metrics of the modeled deposits;
- To compare characteristics of the method against those of other specialized methods.

Firstly, we introduce the subsurface case study and present an overview of the modeling method (section 2, '*Case study and tools*'). Secondly, we illustrate how the method is applied in detail to the chosen examples and the resulting static reservoir models (section 3, 'Modeling and outputs'). Finally, we assess the results through comparisons against corresponding outputs from an industry-standard modeling technique and other more sophisticated tools (section 4, 'Evaluation of results').

2. Case study and tools

2.1 Dataset

To illustrate the proposed workflows for geocellular modeling of fluvial meander-belt reservoirs, the method has been applied to a producing oil reservoir in Western Siberia (Russia). The exact location and stratigraphic context of the reservoir cannot be disclosed because of confidentiality.

The subsurface data employed for constraining the geocellular models consist of a 3D seismic cube and facies logs from uncored wells (Figure 1). Cores are only available from other parts of the succession, but they are believed to sample deposits of similar type to the ones considered here on the basis of analogy in the seismic and well-log data of the intervals.

The part of reservoir being modeled is interpreted as a fluvial succession, based on its stratigraphic context and available sedimentologic evidence (3D seismic, wireline logs). In this succession a segment of channel belt can be interpreted in seismic time slices (Figure 1A). The part of channel belt considered here covers an area of ~ 38 km². In this stretch of meander belt a single sinuous channel fill is observed in seismic, which passes laterally into three fully imaged genetically related point-bar bodies, on the convex side of each channel bend. This unit is therefore interpreted as a simple non-amalgamated channel belt. Portions of partially imaged barform bodies are also recognized; these barforms almost entirely fall outside of the study area. The point-bar bodies are on average ~ 20 m thick, and display km-scale widths, across the channel belt, and lengths, along the channel-belt axis.

The southernmost bar body is the largest one, exhibiting a length of ~ 4.5 km and a width of ~ 3.5 km. The channel fill has a maximum width of ~ 500 m, and a sinuosity of 2.0.

The geomodeling work presented in this study was carried out on two of the three point-bar bodies. The central point-bar body, identified by a frame in Figure 1A, has not been drilled as of November 2017. The northern point-bar body, identified by a star in Figure 1A, has been intersected by 20 vertical wells with an average spacing of less than 400 m; data from eight wells were used in this work (Figure 1B). For the northern point-bar element, facies logs indicate a proportion of sandstone of ~ 80% and a proportion of mudstone of ~ 20%. Cores available from other parts of the succession, and that are thought to represent analogous point-bar deposits, do not contain conglomerates; these cores indicate sand grainsize ranging from fine (dominant) to medium (subordinate). Mudstone beds are resolved on the logs from the northern point-bar body (Figure 1B), which demonstrate an overall fining-upward trend. Some of the uppermost mudstone beds are interpreted to represent bar-top deposits; instead it is envisaged that the mudstone beds contained in the lower and middle section of the element are likely to represent muddy deposits that drape inclined bar-accretion surfaces, because of the position where they occur and by analogy with cored intervals.
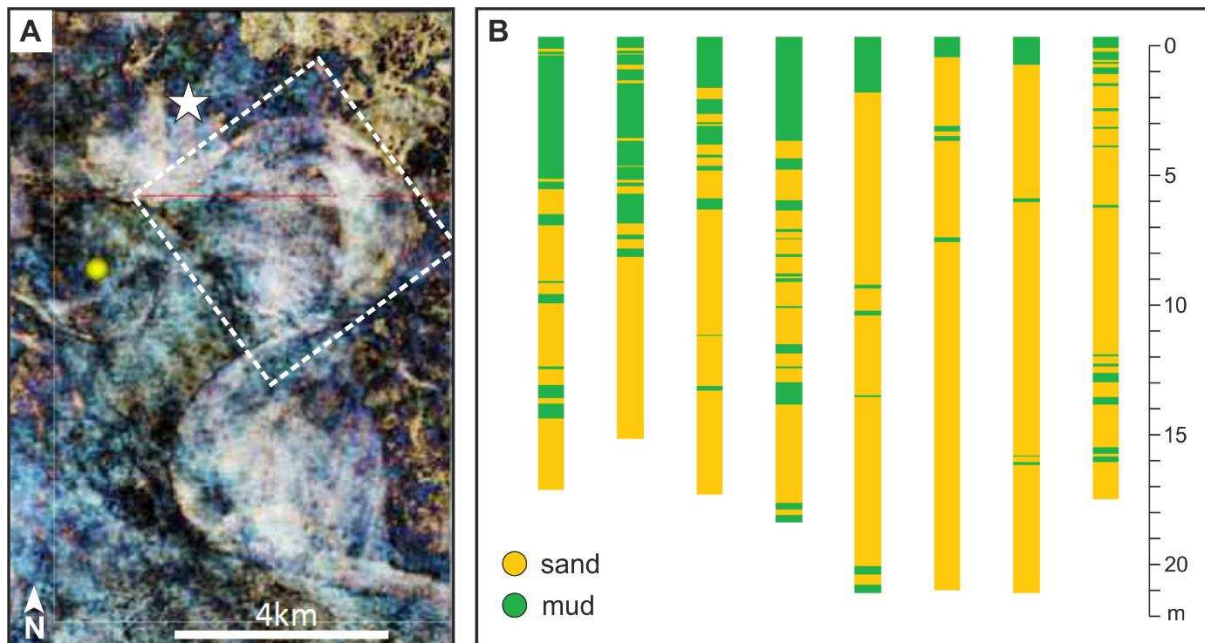
Figure 1: (A) seismic time slice through the meander-belt deposits discussed in the text; the 'central' point-bar unit is contained in the hatched frame; the 'northern' point-bar unit is located by the star. Location and stratigraphic context undisclosed because of confidentiality. (B) Facies logs from eight of the wells drilled in the northern point-bar body; only the interval interpreted as point-bar deposits is represented.

2.2   PB-SAND

The Point Bar Sedimentary Architecture Numerical Deduction (PB-SAND) is a forward numerical model for simulating the sedimentary architecture of fluvial point bars and meander belts (Yan et al.

2017). PB-SAND employs vector-based, grid-free algorithms, whose output can be converted in geocellular grids. PB-SAND simulates deposition and erosion in response to the evolution of meandering channels through a modeling algorithm that is largely geometric, with some process-mimicking techniques. A set of rules are established to enable the user to generate models that incorporate different styles of sedimentary architecture, in relation to different modes of meander transformation (meander expansion and translation, optionally with rotation; Daniel 1971) and to the variable occurrence, distribution and geometry of different facies (see Yan et al., 2017, for details). The output of PB-SAND consists of both deterministic and stochastic solutions: a single deterministic model of planform channel evolution through time is generated for a given input, whereas multiple stochastic realizations of facies architecture can be produced for the same bar geometry. The principles and implementation of PB-SAND are described in greater detail by Yan et al. (2017). Below, a brief overview of model inputs and outputs is provided.

In PB-SAND the modeling workflow is performed in two stages: firstly, the planform evolution of the reach of channel belt being modeled is simulated; secondly, the internal geometry of the point bars is constructed and populated with lithofacies (Yan et al. 2017). The input required by PB-SAND to generate models of planform evolution is the trajectory followed by the meandering channel at a number of significant time steps. The trajectories followed by the migrating channel during the intervals between these time steps are obtained by linear interpolation, in a manner that varies depending on the type of meander transformation being simulated. These interpolated trajectories are then employed by PB-SAND to define point-bar accretion packages. Changing the number of channel trajectories modeled between two time steps will therefore affect the geometry of accretion packages in a certain portion of the point-bar body, and of facies contained therein. PB-SAND models are further constrained on the geometry of the formative river channel, whose maximum depth and width determine the thickness of the bar body and the geometry of accretion surfaces. The internal facies architecture is then built upon the resulting geometric framework, based on constraints consisting of: (i) lithotype rules that specify the presence of certain lithofacies and the position where they occur (e.g., as part of a vertical trend, on accretion surfaces), (ii) overall facies proportions and trends in their distribution (e.g., due to downstream fining toward point-bar-tail areas), (iii) descriptions of the geometries of facies and their boundaries. In subsurface studies, PB-SAND can therefore be constrained using interpreted seismic datasets, which can provide information on channel trajectories and meander-bend transformation, and well data on facies types and characteristics, ideally integrated with insight from geologic analogs or suitable facies models.

The output of PB-SAND consists of vector representations of the facies architecture of point bars and genetically related channel fills, expressed as grids of vertical cross sections that depict the distribution of facies types. These arrays of cross sections can be rendered as raster objects, and subsequently converted to 3D grids whose resolution reflects the spacing and resolution of the cross sections. PB-SAND permits modeling point bars associated with multiple consecutive meander loops; amalgamated but genetically distinct channel belts can also be generated (Yan et al. 2017).

3. Modeling and outputs

3.1 Geomodeling goals and overview

Rule-based reservoir-modeling methods attempt to integrate geologic concepts, implemented as geometric and/or process-oriented operations, with traditional stochastic approaches (Pyrcz et al. 2015). As the scope of PB-SAND is not limited to reservoir-modeling applications (Yan et al. 2017; in press), the goal of this work is to demonstrate how PB-SAND can effectively be applied as a rule-based reservoir-modeling technique for generating complex point-bar facies architectures that reflect geologic understanding.

For hydrocarbon reservoirs composed of large channel belts, of scale similar to the one being discussed here, the workflow is applicable to modeling at field- to sub-field scales. Here, high-resolution sector models are produced for two individual point-bar bodies, which exemplify two different scenarios of subsurface modeling. The application of PB-SAND to the central and northern point-bar bodies is representative of modeling practice undertaken in pre- and post-drill situations, respectively. Geocellular models for the central bar are required as the basis on which to make choices on well design. The modeling workflow applied to the northern point-bar body serves the purpose of demonstrating how a hybrid modeling approach could be implemented to allow effective well conditioning in densely drilled sectors under production.

With regards to both the northern and central reservoir units, it was desirable to understand the impact of the geometry and distribution of intra-point-bar mud-rich deposits on production. The upper mudstone beds recognized in the northern point-bar body (Figure 1B) are interpreted as bar-top deposits. Other mudstone beds occurring throughout the barform are instead thought to drape accretion surfaces that record the migration of the bar front; mudstone units of this type are generally referred to as 'mud drapes' hereafter (cf. McGowen & Gardner 1970; Hartkamp-Bakker & Donselaar 1993; Pranter et al. 2007; Alsop et al. 2014; Biber et al. 2017). Bar-front muds or mud-rich packages might represent different types of deposit with varying characters and genetic significance, some of which might be below the log resolution and are therefore not considered here. The objective is to create models that incorporate bar-front muds of a scale compatible with the cm- to dm-scale thickness observed in the well logs, in consideration of their potential role as baffles or barriers to flow and in view of the need for quantification of their impact on internal compartmentalization of the point-bar bodies.

The proposed modeling strategy employs 3D seismic data to constrain the channel-belt geometry and planform evolution in PB-SAND. Successively, the facies model is built by combining the geometric framework modeled on the seismic with data on the proportion, distribution and geometry of the lithofacies, derived from wells, seismic-attribute maps, and/or geologic analogs. Finally, PB-SAND output grids are post-processed in order to preserve desired geologic features in the final model. These steps, summarized in Figure 2, are illustrated in detail in the three following sections, as applied to create geomodels for the central point-bar body.
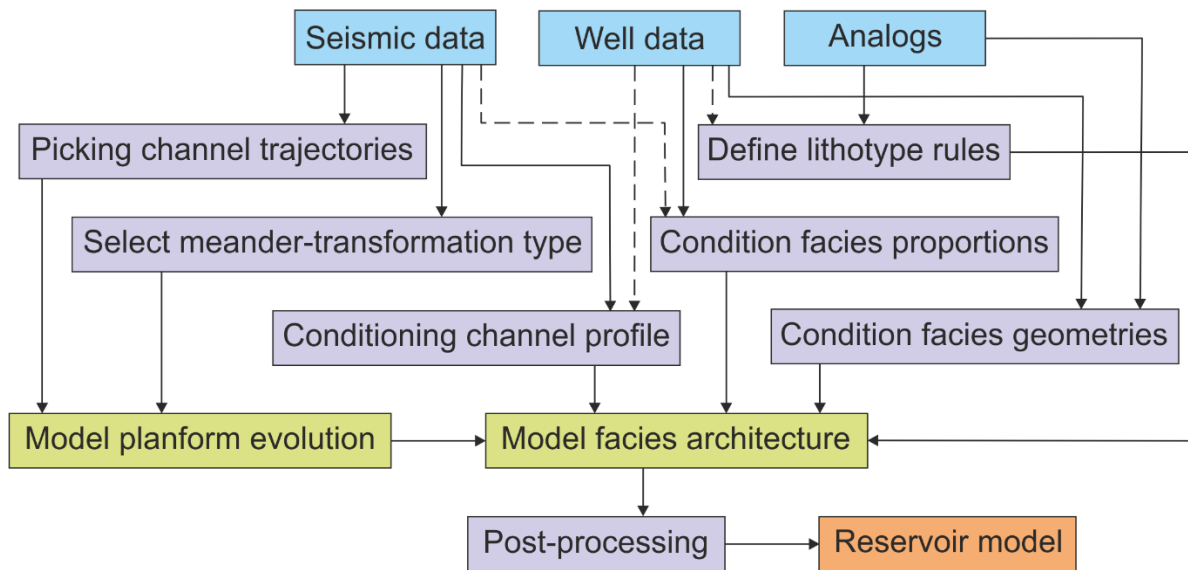
Figure 2: Flow chart of workflows for the creation of static models for large point-bar reservoirs using PB-SAND; boxes represent inputs (blue), operations (purple), and outputs (green). Dashed lines indicate additional routes by which some observations could be used to constrain modeling operations, but that were not followed in the examples presented here.

3.2 Seismic interpretation and planform models

The method relies on the definition of point-bar accretion history based on seismic interpretation. In the dataset used here, inclined accretion surfaces are not identified in cross sections, and, overall, inference of point-bar planform accretion geometries from the seismic dataset is highly uncertain. The southernmost fully imaged bar body provides the most convincing evidence of its internal accretion geometries, and in turn of how its related meander bend might have evolved to produce such architecture. In this sedimentary body, the part adjacent to the inferred inner cut-bank margin comprises stratal packages with relatively constant strike direction, oriented at ~ 20° to the original bank in plan view. This part of the point-bar body is interpreted to have accreted through downstream meander translation (sensu Daniel 1971). The outermost part, by contrast, appears to comprise stratal packages that, in planform, display concavity consistent with that of the associated channel fill to which the bar transitions. This part of the body is interpreted to have accreted through meander expansion (sensu Daniel 1971). Recognition of these different types of meander transformations and related architectural styles can be used to make assumptions with regards to the sedimentary architecture of the two point-bar bodies that occur directly to the north, and which are the only ones for which geocellular modeling was carried out.

The consideration above is useful for establishing a preferred base-case scenario for modeling the point-bar elements, consisting of a phase of meander translation followed by expansion. However, there exists significant uncertainty as to the true internal architecture of the point-bar bodies. As characterizing this form of uncertainty is relevant for development planning, three alternative scenarios of planform evolution are considered for the central point-bar body, consisting of: (i) simple point-bar expansion, (ii) bar expansion and rotation, and (iii) point-bar translation followed by expansion (i.e., the base case). By modeling alternative scenarios of point-bar evolution, the effect of different growth histories on lithologic heterogeneity can be considered. The evolutionary history of

planform development is more apparent in cases where meander bodies possess accretionary geometries that are well imaged on seismic (cf. Maynard & Murray 2003; Fachmi & Wood 2005; Reijenstein et al. 2011; Klausen et al. 2014; Pouderoux et al. 2015; Durkin et al. 2017). In such cases, the planform geometry of accretion packages would be used to constrain the channel trajectories.

The input to PB-SAND for modeling the planform evolution associated with the three scenarios consists of polylines of the river channel trajectories at the three significant time steps. These polylines represent the trajectories taken by the formative river at (i) the time of inception of the channel, triggered for example by river avulsion or meander cut off (initial step, 1), (ii) the time of abandonment of the channel (final step, 3), and (iii) a time step between these two (intermediate step, 2). The trajectory for the final step can be confidently constrained by the centerline of the interpreted abandoned channel fill imaged in the seismic time slice, and is therefore the same for all three scenarios (Figure 3). The trajectories are digitized as vector objects in a GIS environment on georeferenced seismic data, and are imported in PB-SAND as sets of coordinates of points (polyline nodes). By interpolating these trajectories through a number of accretion increments between pairs of time steps, PB-SAND simulates the planform evolution of the point bar (Yan et al. 2017). Multiple transformations of different type that a point bar might experience through time are modeled in successive runs. The three scenarios of planform evolution modeled with PB-SAND for the central point-bar body are shown in Figure 3. These outputs are entirely deterministic.

The three-dimensional expression of the modeled point-bar planform evolution is additionally determined by the hydraulic geometry of the formative channel, defined in terms of maximum depth and width, as inferred here from observations of the thickness of bar deposits and channel-fill width. This output is also deterministic.
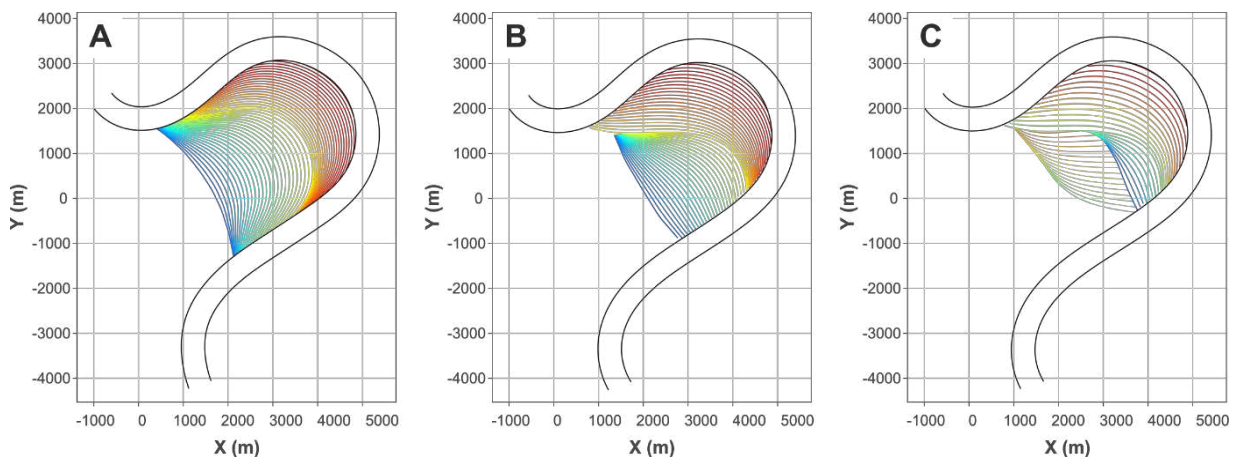

Figure 3: Plan views of three scenarios of planform evolution modeled for the central point-bar body, respectively assuming simple meander expansion (A), expansion and rotation (B), and translation followed by expansion (C). Colored lines represent point-bar accretion surfaces obtained by interpolation of channel trajectories at significant times. Black lines represent the margins of the genetically related channel fill (as imaged in Figure 1A), associated with the youngest channel trajectory used to condition the models. The three channel centerlines used to condition the planform models are represented by: a blue curve (time 1), a yellow curve (time 2), and the centerline of the channel fill (time 3). Two stages of evolution, each including three time steps, were modeled for the scenario in part C.

3.3   Facies distributions

The input to PB-SAND for modeling the distribution of facies in point-bar architectures consists of: (i) lithotype rules, (ii) facies proportions, and (iii) descriptions of facies geometries (Yan et al. 2017).

Similarly to their use in plurigaussian simulations (Armstrong et al. 2011, and references therein), lithotype rules in PB-SAND are used to define the occurrence and position of lithofacies types in the point-bar body. The types of deposits included in a model might represent discrete facies or grainsize classes (e.g., fine sand), or more generic categories (e.g., sand-rich heterolithic deposits). These facies can be arranged in templates that describe their typical vertical juxtaposition. Lateral variations in vertical facies trends across the accretion packages can be reproduced. Facies trends that differ from the overall template can be generated by assigning a component of randomness to vertical facies transitions, through the use of a 'disorder factor' to quantify the variability in facies occurrences across accretion packages. Horizontal trends can also be parameterized, in terms of variations in facies proportions that reflect changes that are commonly known to occur in response to depositional processes. For example, it is possible to force variations in facies proportions that might arise from progressive meander-bend expansion (cf. Wood 1989; van de Lageweg et al. 2014) or at the transition from convex-bench to concave-bench accretion (cf. Nanson & Page 1983; Smith et al. 2011). In this case study, the general lithotype pattern consists of a fining-upward trend: from medium to fine sandstone to bar-top mud; no disorder factor is assigned. Overall proportions of sand and mud are set at 80% and 20%, respectively, to match well observations. For the preferred scenario of planform evolution (point bar translation followed by expansion), all except two simulations are conditioned on increased mud content in point-bar tail areas associated with meander translation, and no facies change through expansion; alternative models are run to take into account scenarios of no facies change at point-bar tail and of increase in mud proportion through bar expansion (Table 1).

PB-SAND additionally permits modeling units that drape the bar fronts with either offlapping or onlapping geometries. Offlapping drape units that taper down the bar front are used to model mud drapes. As opposed to bar-top muds, which, if included, tend to occur over the entire planform area of the bars, mud drapes are localized on accretion surfaces and can be variably discontinuous both down their inclined surfaces and along them. Modeling the occurrence of 'mud drapes' was particularly important for the scopes of this case study. However, these units do not necessarily need to represent individual mudstone beds, in part because this is challenging due to their fine scale and often dense spacing (cf. Novakovic et al. 2002; White 2004; Nardin et al. 2013), and in part because intra-bar compartmentalization might be determined by mud-rich heterolithic packages rather than single mudstone beds (cf. 'fine members' of Thomas et al., 1987), and it might therefore be convenient to model these units instead. Because PB-SAND is grid free, it is possible to create models with mud drapes of virtually any spacing or size; it is however necessary to consider a sensible threshold for units that need to be included in the model, to fulfill the need for a sensible grid size and resolution. Although we may not want or need to expressly include all mud drapes with cm- to dm-scale thickness, an inference on the density of mud drapes that should be modeled can be based on well-log observations and on assumptions of bar-accretion geometries. The minimum spacing chosen for the mud drapes dictates the size of accretion units being modeled in planform.

Additional PB-SAND input describes the geometries of facies contacts and of mud drapes. Facies contacts are described by a Gaussian distribution over which the angles of interdigitation can vary;

parameters that describe these distributions have been kept constant through all simulations. The geometry of mud drapes is described by their thickness, their width along the bar front, from the bar top toward its base, and by their length and horizontal separation along accretion surfaces. These parameters are described by Gaussian distributions. For all the models presented here, all mud drapes are modeled with a constant nominal thickness. The adoption of a constant thickness is driven by the need to maintain the presence and continuity of these features in the final upscaled grid. The choice of thickness values is therefore informed by the desired resolution of the static model. With regards to the other parameters, there is a relative paucity of analog data on intra-point-bar mud-drape geometry, and available data would be of difficult application because their use would need to be reconciled with the fact that we are not planning to model all the mud drapes. The input was chosen to cover a range of parameters that are expected to influence sand connectivity (Table 1). For the base-case planform evolution, seven scenarios of facies architecture have been defined, based on variation of mud-drape frequency, width, length and spacing along channel trajectories (Table 1).

Based on the different scenarios of planform evolution, facies change, and mud-drape characteristics described above, a total of eleven PB-SAND models were run for the central point-bar body (Table 1). For each scenario, multiple equiprobable realizations of facies architecture can be obtained, as PB-SAND allows modeling facies characteristics stochastically (Figure 4).

Table 1: Summary of the main differences between alternative realizations of PB-SAND models for the central point-bar body selected for presentation in this work, expressed as variations relative to a base-case simulation (realization '15', which incorporates mid-range values for all parameters). Although multiple stochastic realizations can be generated with PB-SAND using the same input, in this work a single geocellular model was created for each scenario of planform evolution, facies change, and mud-drape characteristics. Variations in the input parameters are expressed in percentage relative to the base-case simulation ('15').

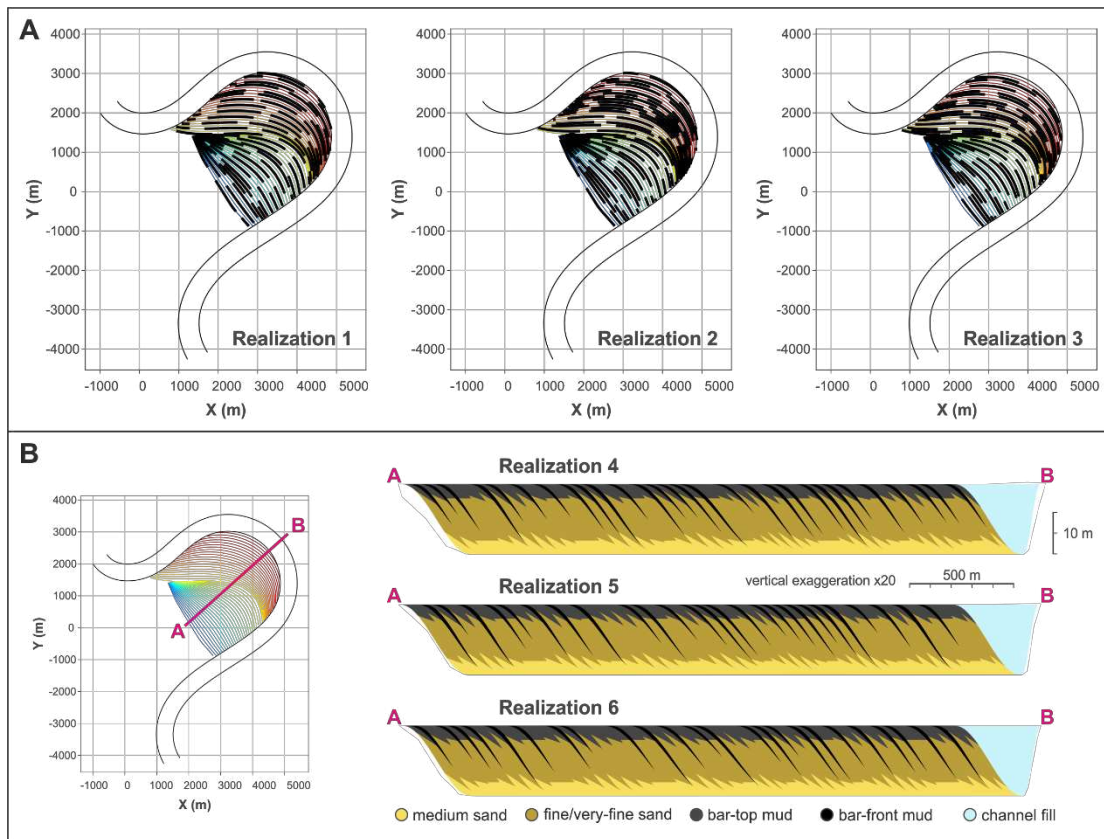| Realization identifier	Rules
15 (base case)	- Meander transformation types: translation followed by expansion - Fining upward: medium sand, to fine and very-fine sand, to mud - Increased mud content at translating point-bar tail (+15% mud) - No change in mud proportion through meander expansion
Realization identifier	**Input variation relative to base-case realization**
16	Increased mud-drape frequency (mean +50%)
17	Decreased mud-drape frequency (mean -67%)
18	Increased mud-drape pinch-out depth, i.e., width along bar front (mean +18%)
19	Decreased mud-drape pinch-out depth, i.e., width along bar front (mean -38%)
20	No change in mud proportion at translating point-bar tail
21	Increased mud proportion through expansion (+9% mud)
22	Decreased along-channel mud-drape length (mean -344%) and spacing (mean -85%)
23	Increased along-channel mud-drape length (mean +105%) and spacing (mean +67%)
24	Simple bar expansion with no translation
25	Bar expansion with slight rotation

Figure 4: Plan views (A) and cross sections (B) of alternative stochastic realizations of facies architecture for the central point-bar body generated using the same input but with different seed numbers, for a scenario of point-bar expansion with rotation. Variations in facies characteristics are expressed in terms of position of mud drapes and geometries of interdigitation of lithotypes. In (A) mud drapes are represented as thick black lines distributed over point-bar accretion surfaces (colored lines), where their extent along accretion surfaces is largest (i.e., toward the bar top).

3.4 Geocellular-grid generation

The output facies models of PB-SAND are exported as 3D geocellular grids, in GSLIB format (Deutsch & Journel 1998). For each model a set of two grids is generated, built from arrays of cross sections oriented orthogonally to each other. This is done to address the fact that mud drapes will not be rendered on cross sections where the local strike direction of accretion surfaces runs parallel to the sections. Sectors from the two output grids in each set are hence merged to ensure that mud-drape geometries are properly incorporated. This operation can be done using a software that permits grid handling, such as SGeMS (Remy et al. 2009).

The eleven grids representing high-resolution sector models produced for the central point-bar body (Figure 5) have vertical and horizontal resolution of 0.18 m and 14 m respectively, for a total grid size between ~ 4.8 and 5.8 million cells (point-bar deposits only). These grids were uspscaled to reduce the grid size to ~ 1.3 to 1.6 million cells, and the vertical resolution to 0.4 m, by following steps of progressive grid coarsening to ensure that facies geometries and bar-front muds were retained in the final grids (Figure 6).

The resulting static models contain characteristics of facies architecture that are evidently non-stationary (e.g., spatial variations in mud-drape geometry and orientation; vertical and horizontal grainsize trends), and that would therefore be comparatively difficult to replicate with traditional geostatistical techniques. Furthermore, the models comprise features with complex curvilinear geometries, whose continuity cannot generally be reproduced using solely pixel-based methods. The set of realizations presented here is being used, in a pre-drill context, to guide development plans for this part of the field, in particular with regards to well orientation and spacing. To this end, the static models are suitable for population with petrophysical properties, in view of their use for dynamic reservoir simulations.
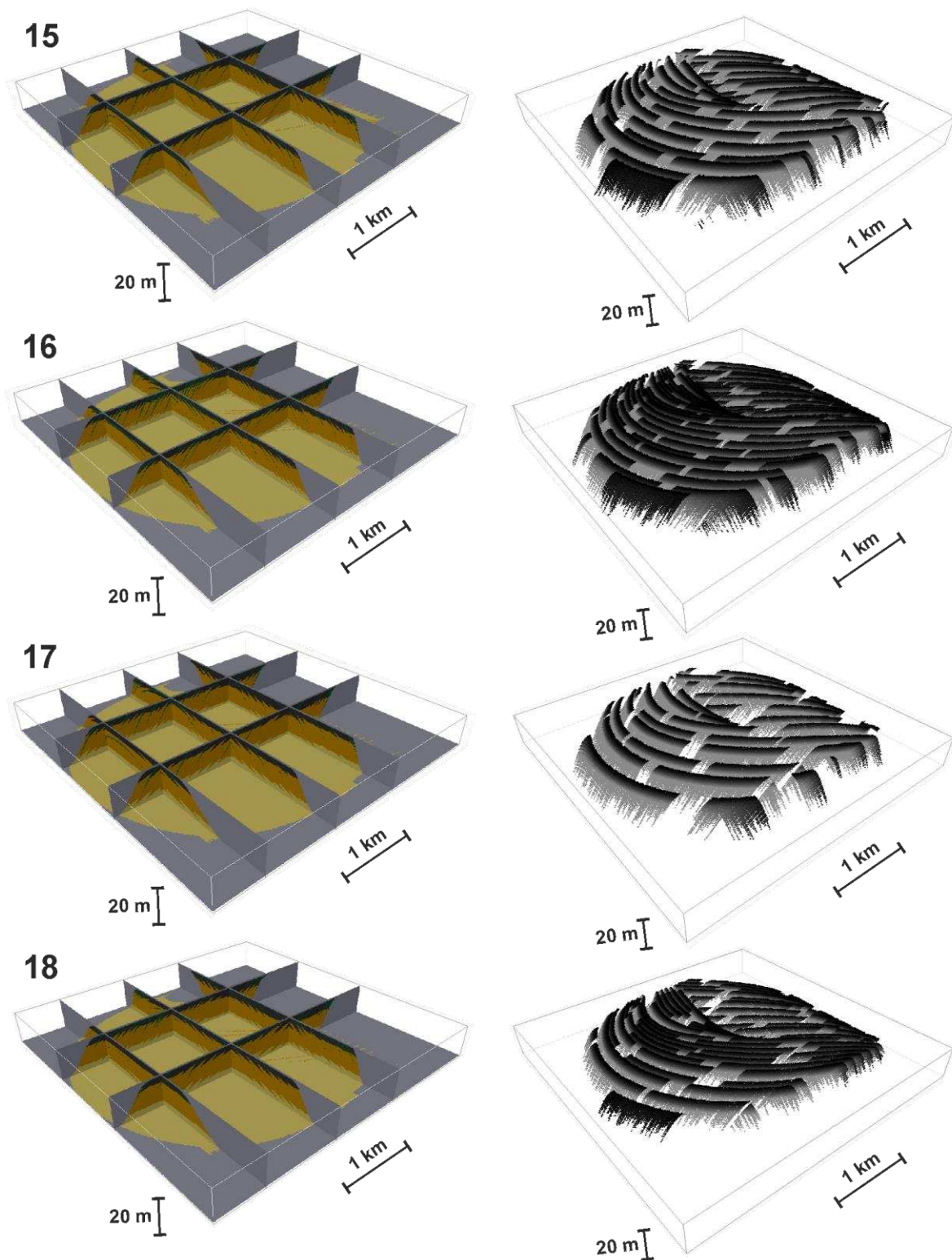
Figure 5: Geocellular models (upscaled grids) for the central point-bar body built using PB-SAND. Fence diagrams of the grids are shown on the left-hand side, coded by facies type. Shaded 3D views of the modeled mud drapes in each simulation are shown on the right-hand side. Numbers denote realizations as in Table 1.
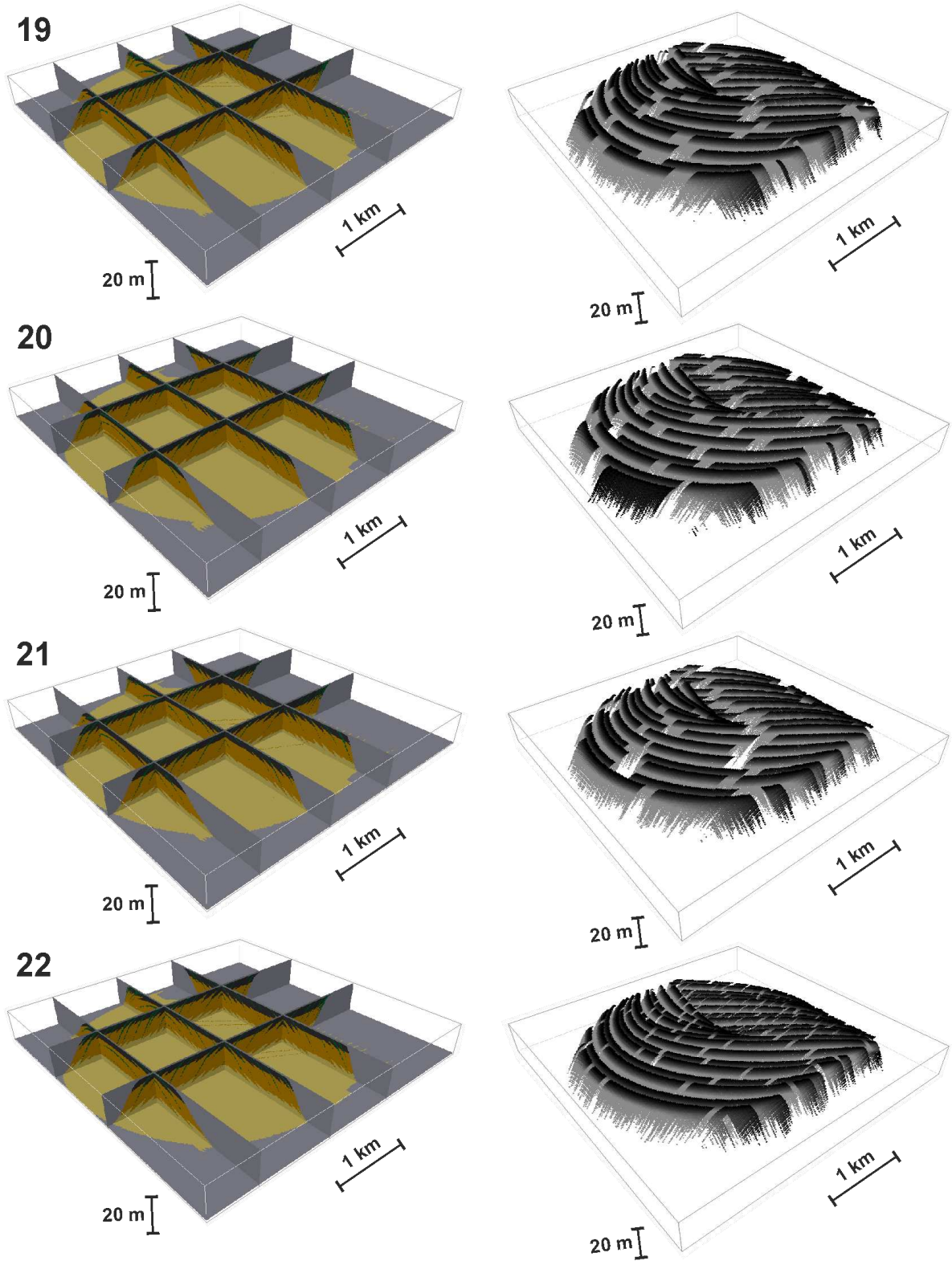
19

20

21

22

Figure 5 (continued).

23

24

25

background facies (overbank and channel fill)
medium sand   bar-top mud
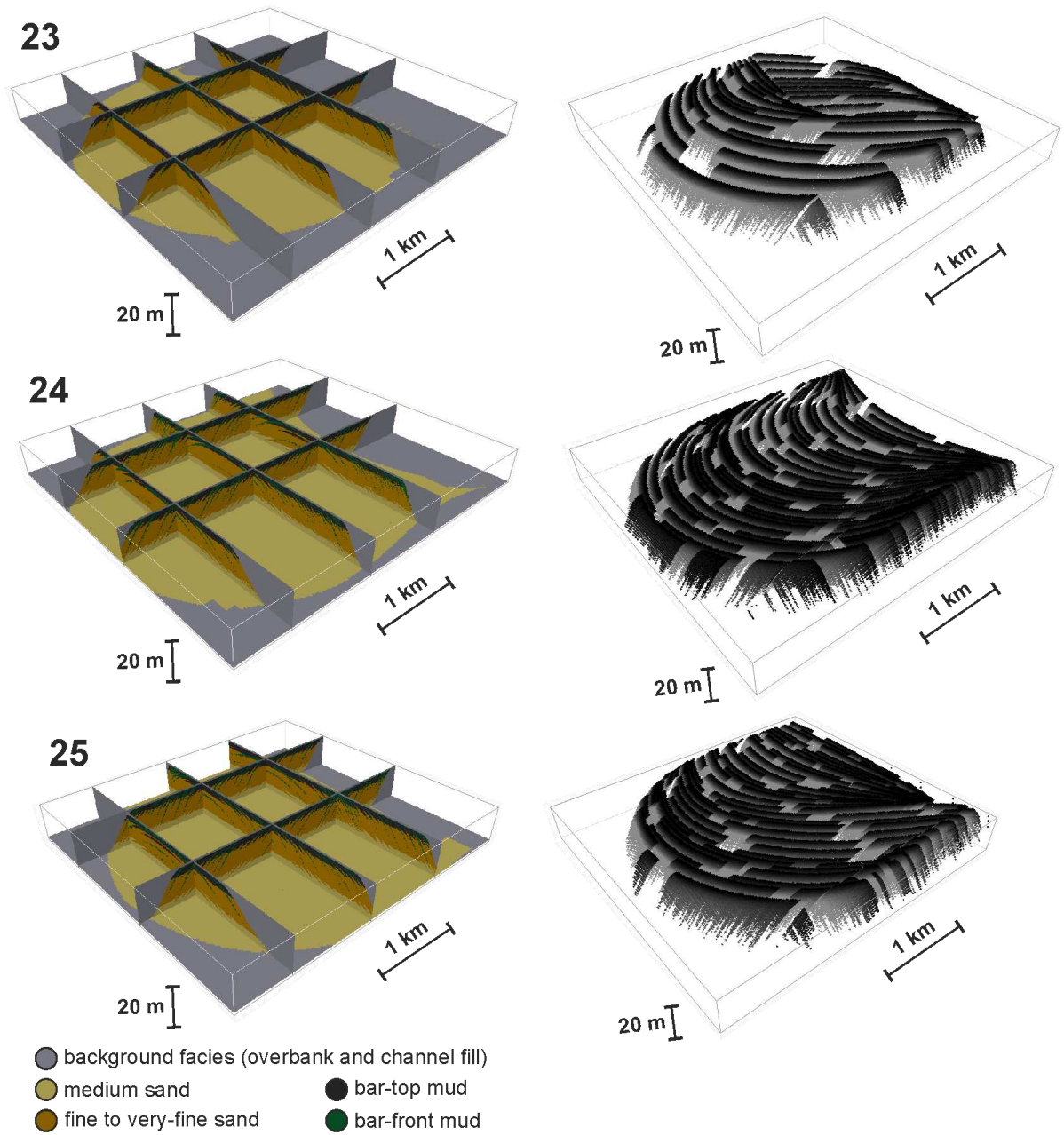fine to very-fine sand   bar-front mud
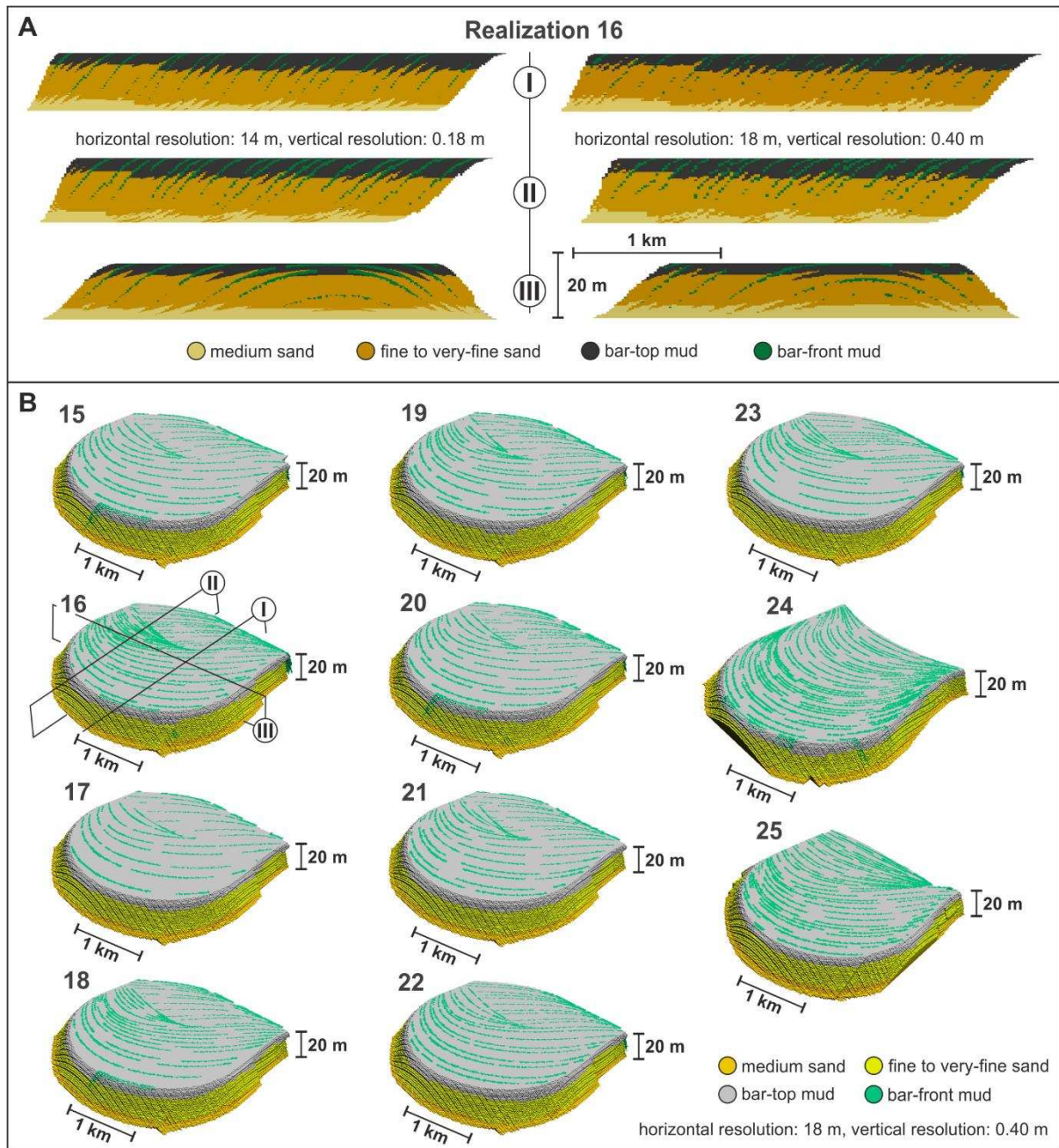
Figure 5 (continued).

Figure 6: (A) Cross sections through a PB-SAND geocellular model (grids at two different resolutions). Higher-resolution sections representing direct PB-SAND outputs are shown on the left; lower-resolution sections obtained through upscaling are shown on the right. (B) Perspective view of the final upscaled grids for the central point-bar body, which maintain the fundamental facies geometries initially modeled with PB-SAND. Roman numerals in (A) identify the position of the cross sections as indicated in (B), for realization 16.

3.5   Soft-data and well conditioning

PB-SAND does not currently allow direct conditioning on wells or on soft data (e.g., seismic attributes). So, the modeling approach outlined above can be readily executed only in cases where models do not need to be conditioned on wells. In situations where matching well data is required, a combined approach can be taken that integrates PB-SAND with traditional geostatistical methods. This approach might be useful in application to densely drilled point-bar reservoirs, particularly those in which the internal accretion geometries are clearly imaged in seismic acquisitions.

This hybrid method was applied to create static models for the northern point-bar body, and again the objective was to generate models that would reflect different scenarios of point-bar evolution and mud-drape characteristics. This approach is essentially hierarchical. PB-SAND can be used to create a geometric framework that honors the seismic dataset. In this framework features such as mud drapes or bar-top facies are used to define regions, within which facies can subsequently be populated using pixel-based methods. This approach entails undertaking all the types of operations described above (in sections 3.2, 3.3, and 3.4) to generate geocellular grids of these lithologic regions. The distribution of lithologic regions can be modeled stochastically using the same functionalities of PB-SAND that enable creation of facies distributions. In the example presented here, mud-drape regions generated by PB-SAND were differentiated from the rest of point-bar deposits so that they would represent areas of increased probability of occurrence of mud. Two scenarios of planform evolution have been considered in this case: (i) simple meander expansion and (ii) downstream translation followed by expansion. Sequential indicator simulations were then run with SISIM (Deutsch & Journel 1998) to simulate the distribution of sand and mud in the point-bar volume. A linear trend of facies probability was used in the vertical direction to recreate a fining-upward trend. The two regions (i.e., mud drapes vs. other facies) were then modeled separately, and the simulations were conditioned on vertical facies logs from eight wells (Figure 7). SISIM was run using median indicator kriging, constrained on a single indicator variogram model that reflects experimental indicator variograms resulting from geostatistical analysis of PB-SAND output; however, the use of a linear trend in facies probability impacted the reproduction of the input indicator variogram model, and therefore of facies continuity. To reduce noise in the realizations, a filter was applied using TRANSCAT (Journel & Xu 1994; Remy et al. 2009). The steps followed to create these models are summarized in Figure 8. An approach of this type could also be taken to permit integration of soft data, such as facies probability maps based on seismic attributes. Other pixel-based approaches, such as methods based on multiple point statistics, could be used in combination with PB-SAND for the same purposes.

This combined approach can be applied to generate detailed geologic models for guiding secondary and enhanced oil recovery from heterogeneous point-bar reservoirs. In this regard, it is particularly important that this method enables the modeling of compartments that might occur in upper point-bar areas because of the presence of bar-front muds of variable geometry and spacing (frequency). The construction of models of this type permits testing scenarios of how the distribution of these deposits might control eventual production. Given the expected impact of mud-drape characteristics on reservoir performance, obtaining a satisfactory history match with this type of modeling approach would likely require multiple modeling iterations with PB-SAND, rather than simply adjusting the sequential simulations.
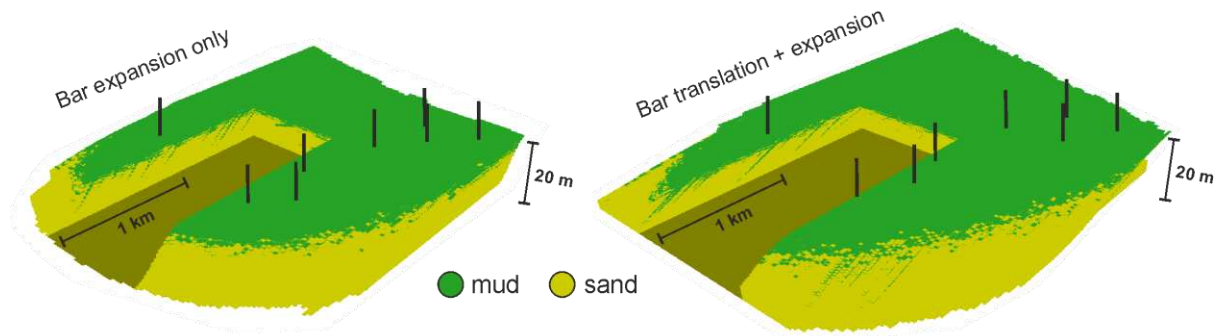
Figure 7: Perspective view of two sector models for the northern point-bar body, built combining PB-SAND with sequential indicator simulations with trends. The realization on the left-hand side incorporates accretion geometries, which define modeling regions, arising from simple bar expansion. The grid on the right-hand side incorporates accretion geometries resulting from bar translation followed by expansion. The position of eight wells used for conditioning the sequential indicator simulations is indicated.

4. Evaluation of results

To assess the value of the proposed approach, geocellular models built using PB-SAND are compared against corresponding outputs from other geomodeling tools that are commonly employed in subsurface characterization (Figure 8). In consideration of the purposes of this work, a comparison is made in terms of metrics that describe the static connectivity of point-bar sands. Furthermore, differences between PB-SAND and other modeling approaches that have been specially created for meander-belt reservoirs are discussed qualitatively.
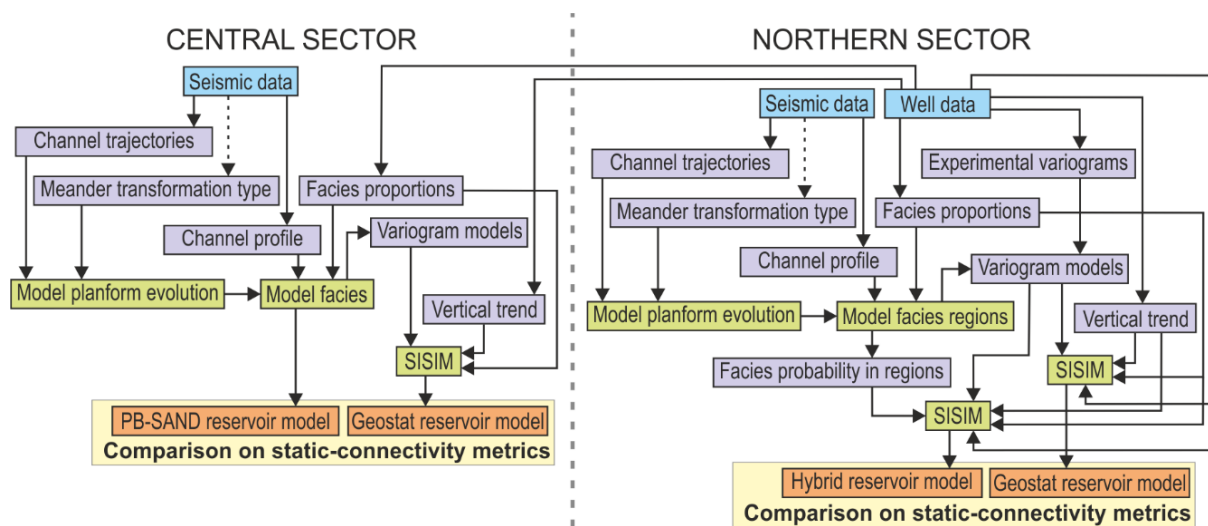

Figure 8: flow charts illustrating the steps followed to create reservoir models using PB-SAND for the central and northern sectors, i.e., in situations of pre- and post-drill modeling (left-hand side and right-hand side, respectively). These steps are explained in detail in sections 3.2 to 3.5. The procedures for creating geostatistical models used as references in the assessment of PB-SAND models are also shown for both cases. Dashed lines indicate that the types of meander transformation could not be constrained unambiguously based on the available seismic data.

18

4.1 Static-connectivity metrics

To model the facies architecture of point-bar reservoirs, a common approach has been the application of variogram-based techniques, sometimes in combination with deterministic approaches or using techniques for reproducing non-stationarity (cf. Novakovic et al. 2002; Li & White 2003; Deschamps et al. 2011; Fustic et al. 2013; Thenin & Larson 2013; Babak et al. 2014; Findlay et al. 2015; Martinius et al. 2017). It is therefore especially useful to compare PB-SAND models with results from pixel-based geostatistical methods. The geocellular models created using PB-SAND for the two examples are compared against a corresponding number of sequential indicator simulations.

Here, eleven sequential indicator simulations (SIS) with trends were run using SISIM (Deutsch & Journel 1998) for the central point bar. The indicator simulations were performed on grids having the same external shape (Figure 6B) and vertical and horizontal resolution as the upscaled PB-SAND models. For a meaningful comparison with the corresponding output from PB-SAND, SIS models were constrained on indicator variogram models that cover the range of experimental variograms for the eleven PB-SAND realizations for the central point bar (Figures 9 and 10). Ranges and model types of the indicator-variogram models employed in SIS are reported in Table 2. In all SIS runs, a vertical linear trend of facies probability was used to reproduce a fining-upward trend. Deterministic means for generating realistic accretion geometries were not used.
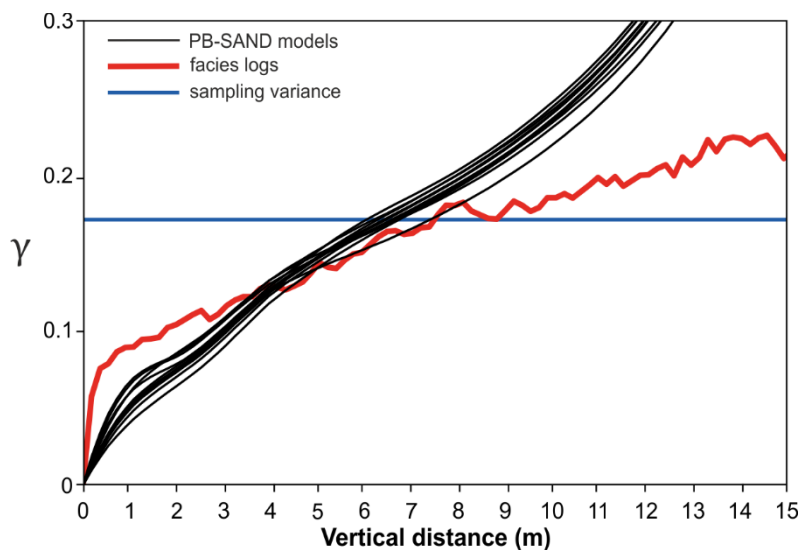

Figure 9: Vertical experimental indicator variograms for the eleven PB-SAND realizations for the central point bar (thin black lines) and for point-bar deposits intersected by the eight wells in the northern point bar (thick red line). A single variogram is computed in each case, because only two facies types (sand, mud) are modeled. The variograms raise above the sampling variance, drawn in blue, i.e., the theoretical sill that would be expected based on the proportions of the two facies types in the case of stationary facies patterns (Ritzi 2000; Gringarten & Deutsch 2001). This likely happens because of non-stationarity in both the facies logs and the geocellular models. Non-stationarity related to common geologic trends known to occur in point-bar deposits, such as fining-upward trends, are directly incorporated in PB-SAND outputs.
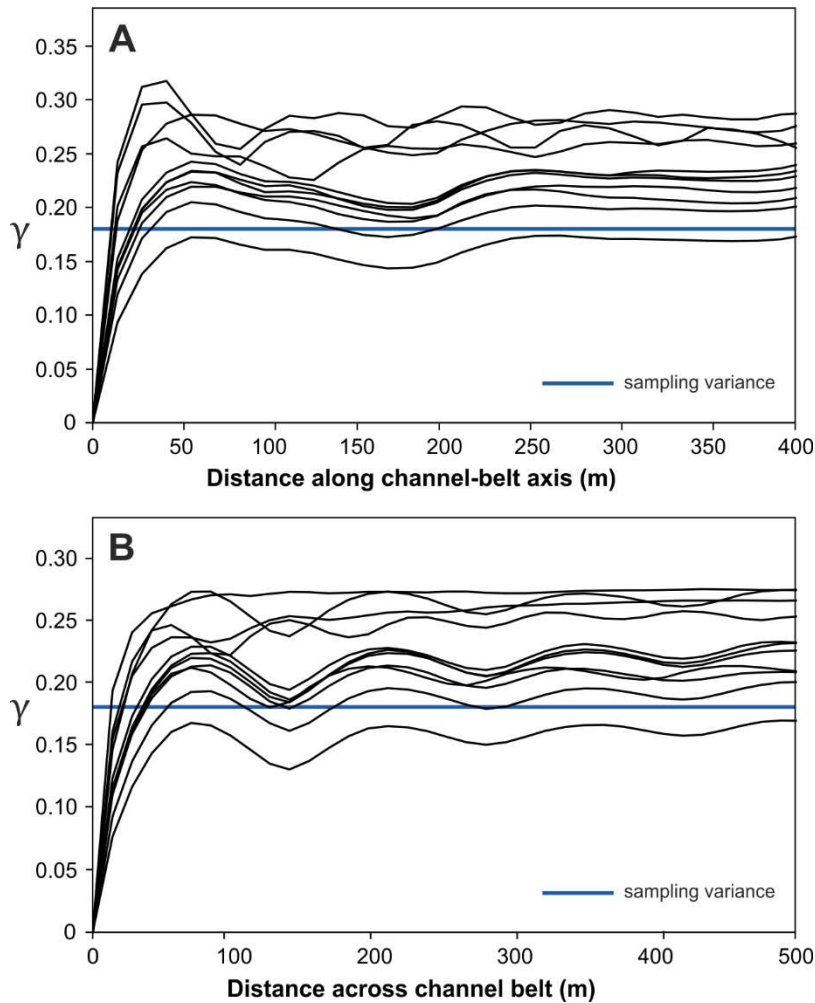
Figure 10: Horizontal experimental indicator variograms for the eleven PB-SAND realizations for the central point bar, computed for directions oriented along (A) and across (B) the channel-belt axis.

Table 2: Input indicator-variogram ranges employed in sequential indicator simulations for comparison against PB-SAND realizations. Eleven spherical indicator variogram models were used, with ranges varying between the minimum and maximum values reported, to match observed experimental indicator variograms of PB-SAND models (Figures 9 and 10); the same value of vertical range was used in all simulations.

Indicator-variogram model parameters			
	Constant	**Minimum**	**Maximum**
Model	Spherical	-	-
Range Z	1 m	-	-
Range X	-	30 m	56 m
Range Y	-	50 m	78 m

Additionally, two SIS models with trends have been created for the northern point-bar body, to enable a comparison of the variability in static connectivity introduced by using PB-SAND to create a

geometric framework, relative to the stochastic variability of equiprobable SIS realizations that can be imposed on that framework.

The central point-bar body was modeled for scopes of development planning, and in particular to guide decisions on well configurations. The adoption of horizontal wells is an increasingly common strategy for producing meander-belt reservoirs (Carter et al. 1998; Balke & Rosauer 2002; Svanes et al. 2004; Wu et al. 2008; Harr et al. 2011; Pakdeesirote et al. 2016; Wang et al. 2016). In heterogeneous point-bar deposits, whether such a strategy is viable and preferable over vertical drilling, and what the ideal well orientation and position might be, are likely determined by accretion geometries and the relative distribution of sand and mud, in addition to the presence and spacing of mud plugs (Colombera et al. 2017). Given that, for the northern point-bar body, a static model is required for guiding production of remaining oil reserves, it is again important to consider the potential control exerted by mud-drape characteristics on the compartmentalization of the uppermost part of the bar. In this comparison we therefore specifically explore the size distribution, connectivity, and estimated tortuosity of sandstone connected components for different sample volumes of upper-bar deposits (Figure 11), and the connectivity of mudstones that might form barriers to flow (cf. Yan et al. in press). Analyses of connectivity metrics associated with PB-SAND and SIS models were undertaken using the computer programs GEO_OBJ (Deutsch 1998) and CONNEC3D (Pardo-Igúzquiza & Dowd 2003).

Connectivity functions express the probability that two cells separated by some distance along a certain direction are connected through cells of the same phase (here, either sand or mud), i.e., they belong to the same 'connected cluster' (Allard & HERESIM Group 1993). Connected clusters represent groups of cells of the same phase that are connected to each other, and their identification varies depending on whether connectivity is considered through cell faces, edges, or corners (Pardo-Igúzquiza & Dowd 2003). For the central point bar, connectivity functions of point-bar muds have been computed based on corner connectivity for the vertical direction. These connectivity functions provide a measure of the vertical connectedness of mudstones that might determine intra-bar compartmentalization (cf. Lajevardi et al. 2015). PB-SAND realizations display a much larger variability in mud connectivity function than seen in models generated using SIS with trends (Figure 12A). It is also seen that, as expected, of the parameters varied in the eleven PB-SAND realizations, the mud-drape pinch-out depth along the bar front has the largest influence on the resulting mud connectivity function (Figure 12A). For the largest connected cluster of sand in the topmost 8 m of each PB-SAND and SIS model, and again considering corner connectivity, the ratio between the cluster surface area and its volume is taken as an estimate of the tortuosity of point-bar sands (Deutsch 1998). PB-SAND realizations for the central point-bar element display larger variability in sand tortuosity than the corresponding SIS models; this might in part relate to the fact that PB-SAND models also display more variable net-sand content in the uppermost 8 m of the bars (Figure 12B).
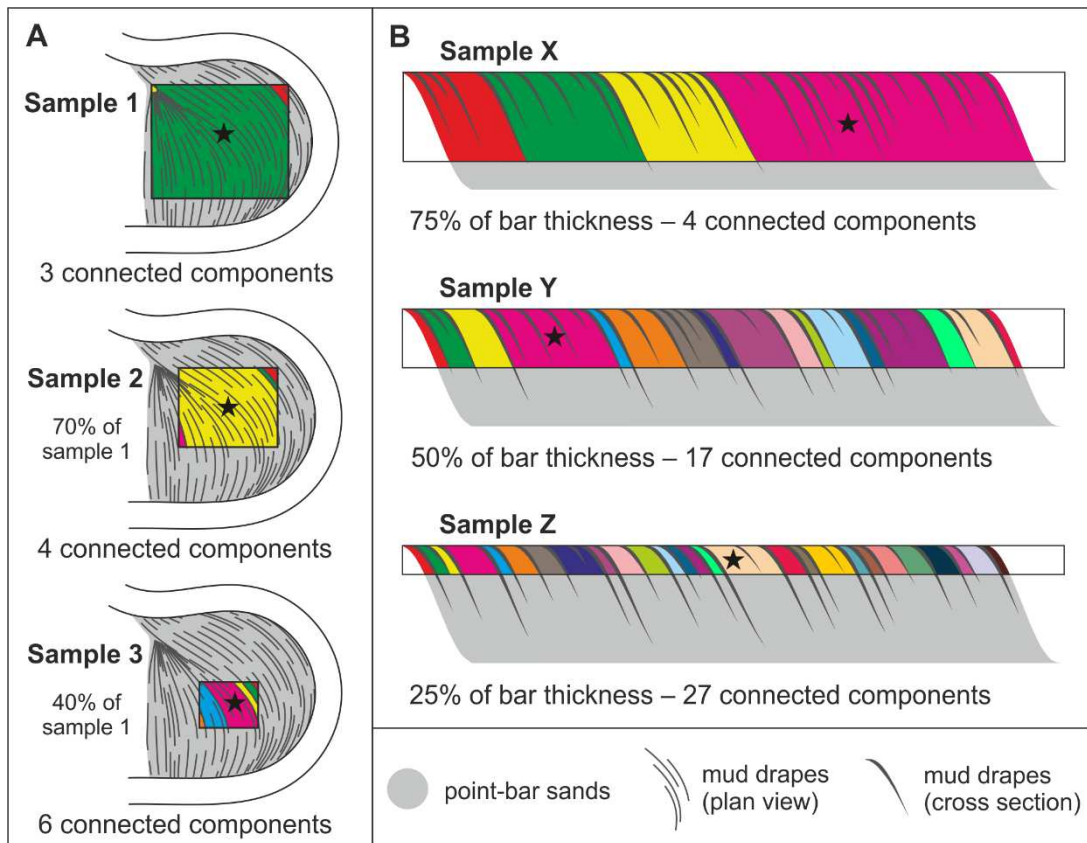
Figure 11: Idealized examples that illustrate the effect of sample size on the number and size of connected components made of point-bar sands that are compartmentalized by mud drapes, in both plan view (A) and cross sections (B). In each sample (black frames), different connected components of point-bar sands are represented as variably colored sectors. The largest connected components in each sample are denoted by stars. Although these examples are depicted as two dimensional sections, in reality all the metrics presented here result from 3D analysis. Analysis of the connectivity of point-bar sands in samples of variable planform and vertical extent allows assessment of the degree at which compartments and dead ends develop at different length-scales.
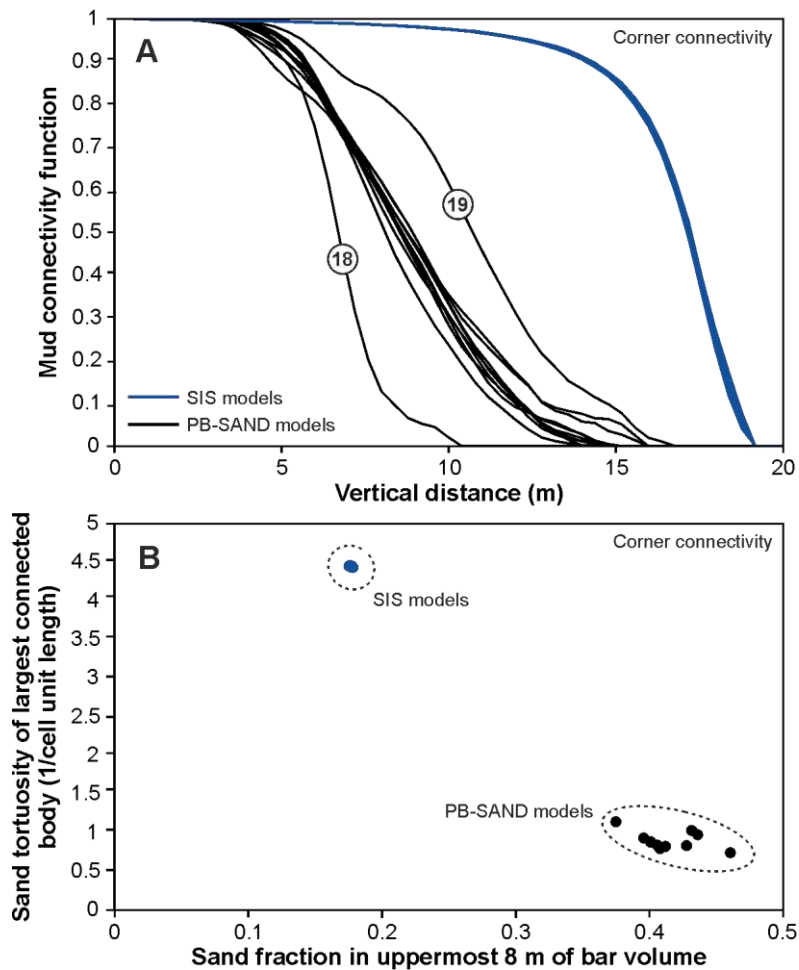
Figure 12: Comparison between PB-SAND models for the central point bar and corresponding SIS realizations, in terms of vertical connectivity function of point-bar muds (A) and estimated sand tortuosity of the largest connected component (cf. Figure 11) versus net sand content for the upper 8 m of point-bar deposits (B). In (A), PB-SAND realizations that express variations in mud-drape pinch-out depth along the bar front ('18' and '19', see Table 1) are associated with the largest variance in mud connectivity function. In all SIS realizations, the limited variability in connectivity metrics is in part related to poor reproduction of the input variogram models due to application of the vertical trend in facies proportions. Higher values of connectivity functions for the SIS models are likely due to the largest overall proportion of mud, as the target fraction was exceeded (~ 30% instead of 20% mud), likely because of the imposed vertical trend. Metrics are based on corner connectivity (i.e., cells that are in touch through their corners, edges, or faces, are considered connected). Whereas the desired non-stationarity in facies distribution can be achieved with both approaches, PB-SAND realizations display significantly higher variability in connectivity metrics.

For models of the northern point bar, connectivity functions of point-bar sands based on face connectivity for directions parallel and orthogonal to the channel-belt axis have been computed. Hybrid models that were built combining PB-SAND with SIS, and that incorporate architecture related to two different scenarios of bar evolution (meander expansion vs translation plus expansion), display a much larger variability in sand connectivity function than what is seen in SIS models that were not constrained on PB-SAND-generated geometries (Figure 13). In particular, the inclusion of geometries associated with both bar expansion and translation determines a reduction in sand connectivity in upper-bar volumes both along and across the channel-belt axis, compared to a scenario

23

of simple expansion. The size distribution of the 30 largest connected clusters of sand in the uppermost 5 m of the modeled bars have also been computed for samples of different size (Figure 14), as a way to characterize the variability in the degree to which compartments and possible dead ends bounded by mud drapes are modeled at different scales. Especially for the largest connected component in each sample, which always contains more than 50% of all sand in the sample, hybrid models that combine PB-SAND and SIS outputs display a larger variability in component size.
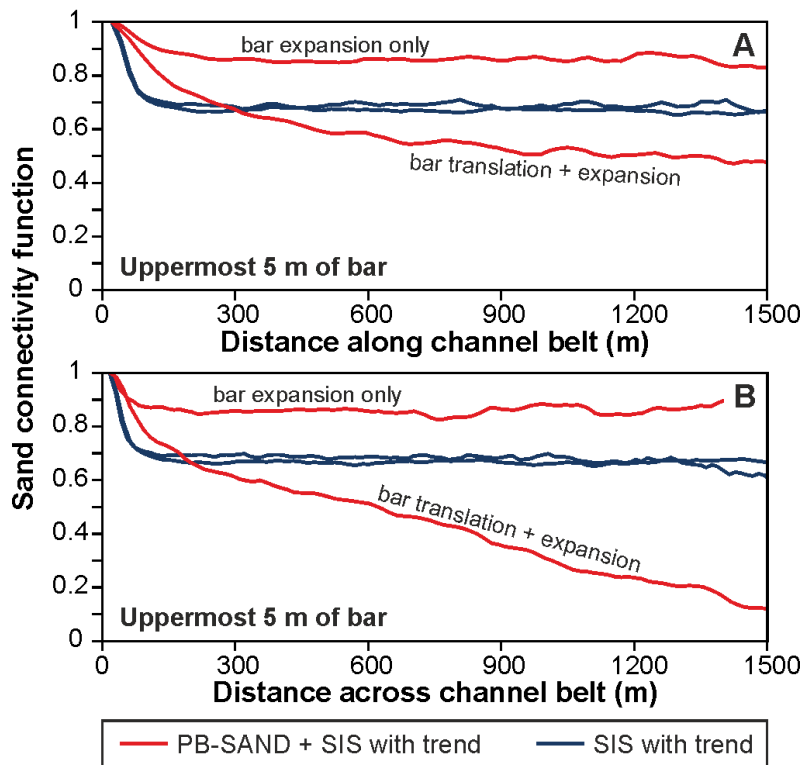

Figure 13: Comparison between the two models for the northern point bar created combining PB-SAND with SIS (red), and two corresponding SIS models that were not conditioned on regions generated with PB-SAND (blue), in terms of horizontal sand connectivity functions. Connectivity functions were computed for directions oriented along (A) and across (B) the channel-belt axis, for the uppermost 5 m of the point-bar body. Metrics are based on face connectivity (i.e., only cells that are in touch through their faces are considered connected). The models that incorporate accretion geometries generated using PB-SAND are characterized by significant difference in connectivity functions, highlighting the importance of accounting for styles of meander growth when modeling facies distributions.
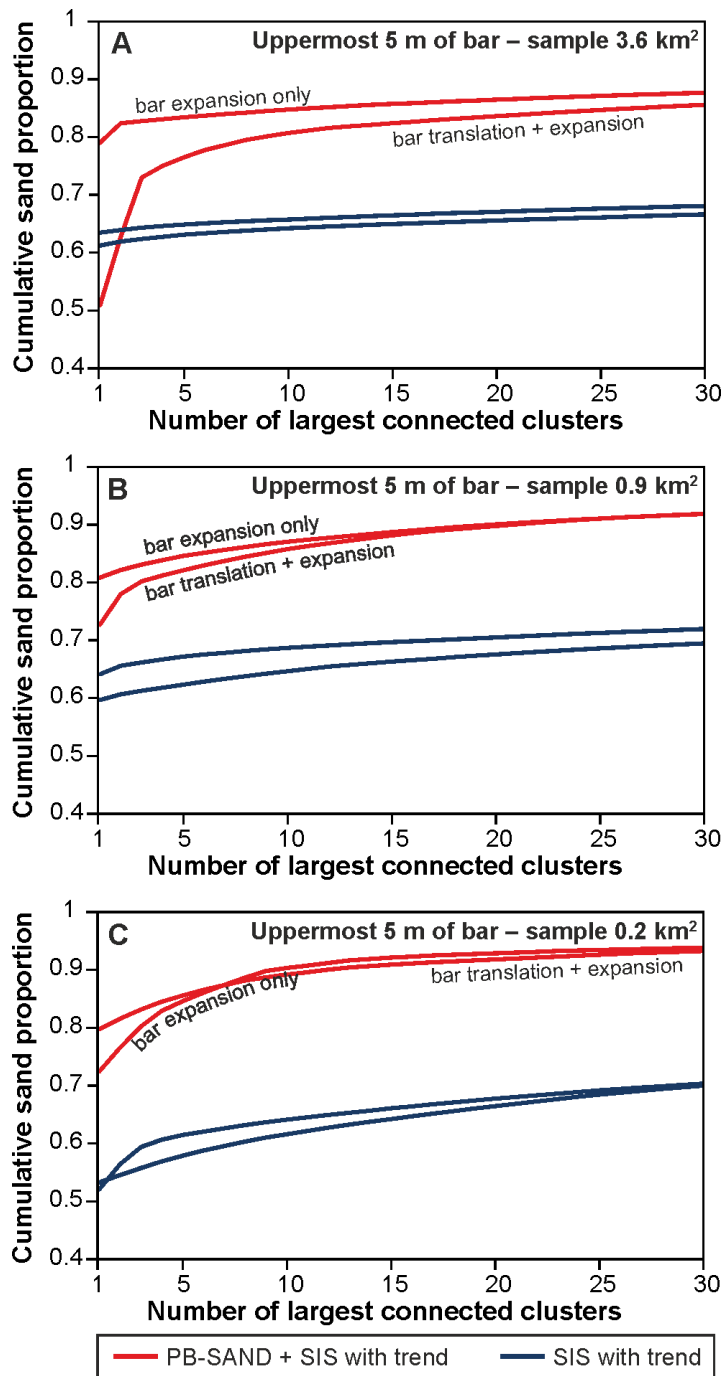
Figure 14: Comparison between the two models for the northern point bar created combining PB-SAND with SIS (red), and two corresponding SIS models that were not conditioned on regions generated with PB-SAND (blue), in terms of cumulative sand proportion in the 30 largest connected clusters of sand, in samples of the uppermost 5 m of the point-bar body. The graphs refer to samples of point-bar volume of variable size, consisting of square planform sectors of 3.6 km^2 (A), 0.9 km^2 (B), and 0.2 km^2 (C) respectively. The large number of connected components recognized in each sample is due to noise inherent in SIS realizations. Metrics are based on face connectivity (i.e., only cells that are in touch through their faces are considered connected).

4.2   Comparison with other methods

In recent years, other specialized methods have been proposed for modeling the facies architecture of fluvial or estuarine point-bar reservoirs (Hassanpour et al. 2013; Li & Wu 2013; Yin 2013; Shu et al. 2015; Ruiu et al. 2016).

Some of these methods allow modeling bar-front muds with object-oriented approaches. Hassanpour et al. (2013) have devised an object-based method that permits modeling bars with simple lobate shapes attached to centerlines. Yin (2013) has instead revised an earlier object-based technique (Deutsch & Tran 2002) for modeling simple sinusoidal channels to allow inclusion of mud drapes in the modeled bar deposits. Crucially, these methods can be conditioned on well data. Some other features of these approaches are likely advantageous in some geomodeling situations: they require a limited number of operations; the geometry of mud drapes can be readily described; stationary outputs suitable as training images for algorithms based on multiple-point statistics can be created. However, both approaches appear to produce geomodels that have limited realism with regards to the desired variability in external bar geometries, styles of accretion, and internal facies distribution. In particular modeling outputs seem to exclusively reflect geometries that result from simple meander expansion. Moreover, these methods cannot be directly conditioned on seismic observations of channel evolution.

Certain surface-based approaches are more similar to PB-SAND, in that they first model channel planform evolutions, which can then be used to constrain characteristics and distribution of point-bar facies. Shu et al. (2015) propose a method that combines a process-mimicking algorithm for inverse simulation of channel centerlines conditioned on the youngest river channel trajectory with a rule-based technique for populating basic point-bar facies (bar sands, lags, mud drapes). A strength of this method lies in its ability to condition mud-drape occurrence on well observations. However, compared to PB-SAND, this approach does not allow users to prescribe specific types of meander transformation, as seen in seismic data, or complex styles of lithologic heterogeneity. Model conditioning requires the definition of parameters that describe boundary conditions that affect river behavior, and the degree to which mud-drape characteristics can be controlled is relatively limited. Ruiu et al. (2016; see also Parquer et al. 2017) also present a surface-oriented approach for modeling the internal and external geometries of meander-belt deposits through simulation of the planform evolution of channel belts. The method generates realistic geometric frameworks that can be translated in static models. It has also been shown that using this method of simulation of facies distributions can be achieved with consideration of channel dynamics and their geologic controls (cf. Rongier et al. 2017, for an application to the deposits of submarine channels). Processes of meander translation, expansion and rotation can all be modeled. However, in the basic form of the modeling method, simulation of these processes has not yet been linked to the generation of distinct styles of internal facies architecture. Outputs cannot currently be conditioned on wells.

All modeling approaches that have been specially created for modeling point-bar reservoirs have pros and cons, and each of them is effectively designed to fulfill specific modeling requirements. The main advantages of PB-SAND over other approaches lie in its abilities to: (i) effectively consider multiple user-specified types of meander-bend evolution, (ii) link types of meander evolution to facies organization while maintaining flexible rules for lithologic heterogeneity, and (iii) be conditioned on seismic interpretations. PB-SAND, as presently implemented, is a valuable tool for modeling large point-bar elements that are imaged in seismic, particularly in pre-drill scenarios.

5. Summary and conclusions

Detailed sector models are commonly required to guide development plans, sometimes with the aim of assessing the impact upon reservoir depletion of mud-prone units that form potential baffles or barriers to flow (cf. Larue & Legarre 2004; Chapin et al. 2014; Mulder & Tinedo 2015; Ainsworth et al. 2016). For fluvial point-bar reservoirs, geologic realism in static models of this type requires consideration of how meander-bend evolution determines geometries and distribution of lithofacies.

Here, a proof-of-concept application is presented to show how a forward stratigraphic modeling tool, PB-SAND, can leverage seismic interpretations to achieve realistic facies distributions in high-resolution geomodels of point-bar reservoirs. The suggested approach is therefore applicable in cases of fluvial reservoirs made of seismic-scale bars, with km-scale lateral extent (e.g., Labrecque et al., 2011; Martinius et al., 2017), which are common in settings favorable to the development of large rivers, such as on continental shelves that are exposed at lowstand (cf. Posamentier 2001; Miall 2002; Darmadi et al. 2007; Reijenstein et al. 2011; Alqahtani et al. 2015) or close to the margins of continental interiors with very large drainage areas (e.g., Triassic Mungaroo Formation, North West Shelf of Australia; Cretaceous Grand Rapids and McMurray formations, Alberta, Canada; Paleocene Wilcox Group, Texas, USA; Lewis & Sircombe 2013; Blum & Pecha 2014). PB-SAND permits the integration of subsurface data with insight gained from geologic analogs, and to infuse sedimentologic process understanding of lithologic organization through a rule-based approach, to explore different scenarios of point-bar reservoir architecture for development purposes. The suggested modeling workflow is particularly useful for reservoir assessment in pre-drill situations, but can also be coupled with common geostatistical techniques to make static models honor well data.

Overall, the results presented here indicate that constructing point-bar reservoir models using PB-SAND permits a more direct control on the reproduction of geologic features that are important in affecting the static connectivity of net-reservoir volumes (distribution and characteristics of mud drapes, mud-prone packages), compared to traditional variogram-based methods.

The approach presented here can be improved in a number of aspects: PB-SAND is being revised to further improve the geologic realism of its outputs and to facilitate its use. Significant improvements can be achieved by honing the code to permit: (i) simulation of variations in bar thickness in relation to variations in channel depth along its length and through time as meanders evolve (cf. Willis & Tang 2010), (ii) simulation of multiple types of evolution in a single run, (iii) creation of models for many (i.e., more than three) consecutive meander loops, (iv) consideration of spatio-temporal trends in the distribution of mud drapes (e.g., downstream or lateral increase in mud-drape density and size within a point-bar unit; cf. Wood 1989; Wightman & Pemberton 1997; Deschamps et al. 2011), (v) direct well conditioning. It would also be convenient to streamline the different modeling operations, which are currently performed with different software tools, by implementing all required software in the same platform.

This novel approach of drawing geometries from surfaces imaged in seismic data and linking the facies architecture of the packages they bound to geologic concepts by means of rule-based practice can likely be extended to other geologic settings.

Acknowledgments

References

Ainsworth, R. B., Payenberg, T. H. D., Willis, B. J., Sixsmith, P. J., Yeaton, J. W., Sykiotis, N., & Lang, S. C. (2016). Predicting shallow marine reservoir heterogeneity using a high resolution mapping approach, Brigadier Formation, NWS, Australia. Society of Petroleum Engineers Asia Pacific Oil & Gas Conference and Exhibition, Perth, Australia, 25-27 Oct., SPE 182355.

Allard, D., & HERESIM Group (1993). On the connectivity of two random set models: the truncated Gaussian and the Boolean. In: Soares, A. (ed.) Geostatistics Tróia'92, Springer, Dordrecht, 467-478.

Alqahtani, F. A., Johnson, H. D., Jackson, C. A.-L., & Som, M. R. B. (2015). Nature, origin and evolution of a Late Pleistocene incised valley-fill, Sunda Shelf, Southeast Asia. Sedimentology, 62, 1198-1232.

Alsop, D. B., Al Ghammari, M., Al Abri, A., Al Mahrooqi, A., Al Rawahi, H., & Salem, H. (2014). Reservoir architecture of the Gharif Formation outcrops in the Southern Huqf area, Sultanate of Oman. In: Martinius, A. W., Howell, J. A., & Good, T. R. (eds.) Sediment-Body Geometry and Heterogeneity: Analogue Studies for Modelling the Subsurface, Geological Society, London, Special Publications, 387, 111-133.

Armstrong, M., Galli, A., Beucher, H., Loc'h, G., Renard, D., Doligez, B., Eschard, R., & Geffroy, F. (2011). Plurigaussian simulations in geosciences. Springer, Berlin, 176 pp.

Babak, O., Bergey, P., & Deutsch, C. V. (2014). Facies trend modeling for SAGD application at Surmont. Journal of Petroleum Science and Engineering, 119, 85-103.

Balke, S. C., & Rosauer, M. S. (2002). Real time, real fast: drilling horizontal wells in a heavy oil environment. Society of Petroleum Engineers International Thermal Operations and Heavy Oil Symposium and International Horizontal Well Technology Conference, Calgary, Alberta, Canada, 4-7 Nov., SPE/Petroleum society of CIM/CHOA 78954.

Biber, K., Khan, S. D., Bhattacharya, J. P., Barton, M. D., & Glennie, C. L. (2017). Quantitative characterization of shales within tidally influenced fluvial valley fill deposits of the Ferron Sandstone, eastern Utah: Implications for hydrocarbon exploration. AAPG Bulletin, 101, 1599-1623.

Bluck, B. J. (1971). Sedimentation in the meandering River Endrick. Scottish Journal of Geology, 7, 93-138.

Blum, M., & Pecha, M. (2014). Mid-Cretaceous to Paleocene North American drainage reorganization from detrital zircons. Geology, 42, 607-610.

Carter, D. C. (2003). 3-D seismic geomorphology: Insights into fluvial reservoir deposition and performance, Widuri field, Java Sea. AAPG Bulletin, 87, 909-934.

Carter, D. C., Kortlang, W., Smelcer, M., & Troncoso, J. C. (1998) An integrated approach to horizontal well design and planning in Widuri Field, offshore southeast Sumatra, Indonesia. Indonesian Petroleum Association, 26th Annual Convention Proceedings, 2, 135-162.

Chapin, M. A., & Mayer, D. F. (1991). Constructing a three-dimensional rock-property model of fluvial sandstones in the Peoria field, Colorado. In: Miall, A. D., & Tyler, N. (eds.) The three-dimensional facies architecture of terrigenous clastic sediments and its implications for hydrocarbon discovery and recovery, SEPM (Society for Sedimentary Geology) Concepts in Sedimentology and Paleontology, 3, 160-171.

Chapin, M. A., Brandon, N. W., Ugueto, G., Bobich, J. K., Fleming, C. H., Diomampo, G. P., Schiller, H. L., Hurd, S. M., Brandon, N. W., Ugueto, G., & Fleming, C. H. (2014). Integrated static and dynamic modeling of the Pinedale tight gas field, Wyoming. In: Longman, M., Kneller, S., Meyer, T., & Chapin, M. (eds.) Pinedale field: case study of a giant tight gas sandstone reservoir, AAPG Memoir 107, 497-531.

Colombera, L., Mountney, N. P., McCaffrey, W. D. (2012a). A relational database for the digitization of fluvial architecture: Concepts and example applications. Petroleum Geoscience, 18, 129-140.

Colombera, L., Felletti, F., Mountney, N. P., & McCaffrey, W. D. (2012b). A database approach for constraining stochastic simulations of the sedimentary heterogeneity of fluvial reservoirs. AAPG Bulletin, 96, 2143-2166.

Colombera, L., Mountney, N. P., Russell, C. E., Shiers, M. N., & McCaffrey, W. D. (2017). Geometry and compartmentalization of fluvial meander-belt reservoirs at the bar-form scale: quantitative insight from outcrop, modern and subsurface analogues. Marine and Petroleum Geology, 82, 35-55.

Cornish, F. G. (1984). Fluvial environments and paleohydrology of the Upper Morrow 'A' (Pennsylvanian) meander belt sandstone, Beaver County, Oklahoma. Shale Shaker, 34, 70-80.

Daniel, J. F. (1971). Channel movement of meandering Indiana streams. US Government Printing Office. U.S. Geological Survey, Professional Paper 732A, 18 pp.

Darmadi, Y., Willis, B. J., & Dorobek, S. L. (2007). Three-dimensional seismic architecture of fluvial sequences on the low-gradient Sunda Shelf, offshore Indonesia. Journal of Sedimentary Research, 77, 225-238.

de Rooij, M., Corbett, P. W., & Barens, L. (2002). Point bar geometry, connectivity and well test. First Break, 20, 755-763.

Deschamps, R., Guy, N., Preux, C., & Lerat, O. (2011). Impact of Upscaling on 3-D Modelling of SAGD in a Meander Belt. Society of Petroleum Engineers Annual Technical Conference and Exhibition, Denver, Colorado, USA, 30 Oct.-2 Nov., SPE 147035.

Deutsch, C. V. (1998). Fortran programs for calculating connectivity of three-dimensional numerical models and for ranking multiple realizations. Computers & Geosciences, 24, 69-76.

Deutsch, C. V., & Journel, A. G. (1998). Geostatistical software library and user's guide. Oxford University Press, New York, 368 pp.

Deutsch, C. V., & Tran, T. T. (2002). FLUVSIM: a program for object-based stochastic modeling of fluvial depositional systems. Computers & Geosciences, 28, 525-535.

Durkin, P. R., Boyd, R. L., Hubbard, S. M., Shultz, A. W., & Blum, M. D. (2017) Three-Dimensional Reconstruction of Meander-Belt Evolution, Cretaceous McMurray Formation, Alberta Foreland Basin, Canada. Journal of Sedimentary Research, 87, 1075-1099.

Edie, R. W., & Andrichuk, J. M. (2005). Meander belt entrapment of hydrocarbons, Campbell-Namao Field, Alberta. AAPG Search & Discovery Article #20027.

El-Mowafy, H. Z., & Marfurt, K. J. (2016). Quantitative seismic geomorphology of the middle Frio fluvial systems, south Texas, United States. AAPG Bulletin, 100, 537-564.

Ethridge, F. G., & Schumm, S. A. (2007). Fluvial seismic geomorphology: a view from the surface. In: Davies, R. J., Posamentier, H. W., Wood, L. J., & Cartwright, J. A. (eds.) Seismic geomorphology: applications to hydrocarbon exploration and production. Geological Society, London, Special Publications, 277, 205-222.

Fachmi, M., & Wood, L. J. (2005). Seismic geomorphology: a study from West Natuna Basin, Indonesia. Indonesian Petroleum Association, 30th Annual Convention Proceedings, 1, 163-178.

Feng, Z. Q. (2000). An investigation of fluvial geomorphology in the Quaternary of the Gulf of Thailand, with implications for river classification. Doctoral dissertation, University of Reading, UK, 198 pp.

Findlay, D., Nardin, T., Wright, A., & Mojarad, R. S. (2015) Modeling lateral accretion in McMurray Formation fluvial-estuarine channel systems: Grizzly Oil Sands' May River SAGD project, Athabasca. AAPG Search & Discovery Article #41611.

Fustic, M., Hubbard, S. M., Spencer, R., Smith, D. G., Leckie, D. A., Bennett, B., & Larter, S. (2012). Recognition of down-valley translation in tidally influenced meandering fluvial deposits, Athabasca Oil Sands (Cretaceous), Alberta, Canada. Marine and Petroleum Geology, 29, 219-232.

Fustic, M., Thurston, D., Al-Dliwe, A., Leckie, D. A., & Cadiou, D. (2013). Reservoir modeling by constraining stochastic simulation to deterministically interpreted three-dimensional geobodies: case study from Lower Cretaceous McMurray Formation, Long Lake steam-assisted gravity drainage project, Northeast Alberta, Canada. In: Hein, F. J., Leckie, D., Larter, S., & Suter, J. R. (eds.) Heavy-oil and oil-sand petroleum systems in Alberta and beyond, AAPG Studies in Geology, 64, 565-604.

Gorain, S. & Shalivahan (2018) Application of attribute-based inversion and spectral decomposition with red–green–blue colour blending for visualization of geological features: a case study from the Kalol Field, Cambay Basin, India. Petroleum Geoscience24, 102-111.

Gringarten, E., & Deutsch, C. V. (2001). Teacher's aide: variogram interpretation and modeling. Mathematical Geology, 33, 507-534.

Harr, M. S., Chokasut, S., Bhuripanyo, C., Viriyasittigun, P., & Harun, A. R. (2011) Evaluation of factors in horizontal well recovery in the Pattani Basin in the Gulf of Thailand. International Petroleum Technology Conference, IPTC, 14981.

Hartkamp-Bakker, C. A., & Donselaar, M. E. (1993). Permeability patterns in point bar deposits: Tertiary Loranca Basin, central Spain. In: Flint, S. S., & Bryant, I. D. (eds.) The geological modelling of hydrocarbon reservoirs and outcrop analogues, IAS Special Publication 15, 157-168.

Hassanpour, M. M., Pyrcz, M. J., & Deutsch, C. V. (2013). Improved geostatistical models of inclined heterolithic strata for McMurray Formation, Alberta, Canada. AAPG Bulletin, 97, 1209-1224.

Hubbard, S. M., Smith, D. G., Nielsen, H., Leckie, D. A., Fustic, M., Spencer, R. J., & Bloom, L. (2011). Seismic geomorphology and sedimentology of a tidally influenced river deposit, Lower Cretaceous Athabasca oil sands, Alberta, Canada. AAPG Bulletin, 95, 1123-1145.

Journel, A. G., & Xu, W. (1994). Posterior identification of histograms conditional to local data. Mathematical Geology, 26, 323-359.

Klausen, T. G., Ryseth, A. E., Helland-Hansen, W., Gawthorpe, R., & Laursen, I. (2014). Spatial and temporal changes in geometries of fluvial channel bodies from the Triassic Snadd Formation of offshore Norway. Journal of Sedimentary Research, 84, 567-585.

Labrecque, P. A., Hubbard, S. M., Jensen, J. L., & Nielsen, H. (2011). Sedimentology and stratigraphic architecture of a point bar deposit, Lower Cretaceous McMurray Formation, Alberta, Canada. Bulletin of Canadian Petroleum Geology, 59, 147-171.

Lajevardi, S., Babak, O., & Deutsch, C. V. (2015). Estimating barrier shale extent and optimizing well placement in heavy oil reservoirs. Petroleum Geoscience, 21, 322-332.

Larue, D. K., & Legarre, H. (2004). Flow units, connectivity, and reservoir characterization in a wave-dominated deltaic reservoir: Meren reservoir, Nigeria. AAPG Bulletin, 88, 303-324.

Lewis, C. J., & Sircombe, K. N. (2013). Use of U-Pb geochronology to delineate provenance of North West Shelf sediments, Australia. In: Keep, M., & Moss, S. J. (eds.) The sedimentary basins of Western Australia IV: Proceedings of the Petroleum Exploration Society of Australia Symposium, 1-27.

Li, H., & White, C. D. (2003). Geostatistical models for shales in distributary channel point bars (Ferron Sandstone, Utah): From ground-penetrating radar data to three-dimensional flow modeling. AAPG Bulletin, 87, 1851-1868.

Li, Y., & Wu, S. (2013). Hierarchical nested simulation approach in reservoir architecture modeling. Petroleum Exploration and Development, 40, 676-681.

Martinius, A. W., Fustic, M., Garner, D. L., Jablonski, B. V. J., Strobl, R. S., MacEachern, J. A., & Dashtgard, S. E. (2017). Reservoir characterization and multiscale heterogeneity modeling of inclined heterolithic strata for bitumen-production forecasting, McMurray Formation, Corner, Alberta, Canada. Marine and Petroleum Geology, 82, 336-361.

Maynard, J. R., Feldman, H. R., & Alway, R. (2010). From bars to valleys: the sedimentology and seismic geomorphology of fluvial to estuarine incised-valley fills of the Grand Rapids Formation (Lower Cretaceous), Iron River Field, Alberta, Canada. Journal of Sedimentary Research, 80, 611-638.

Maynard, K., & Murray, I. (2003). One million years from the Upper Arang Formation, West Natuna Basin, implications for reservoir distribution and facies variation in fluvial deltaic deposits. Indonesian Petroleum Association, 29th Annual Convention Proceedings, 1, 270-276.

McGowen, J. H., & Garner, L. E. (1970). Physiographic features and stratification types of coarse-grained point bars: modern and ancient examples. Sedimentology, 14, 77-111.

Miall, A. D. (2002). Architecture and sequence stratigraphy of Pleistocene fluvial systems in the Malay Basin, based on seismic time-slice analysis. AAPG Bulletin, 86, 1201-1216.

Mulder, R., & Tinedo, C. (2015). Geomodeling workflow adapted to a mature extra heavy oilfield. Case study: modelization of Petrocedeño deltaic reservoir for the EOR polymer project. Society of Petroleum Engineers Latin American and Caribbean Petroleum Engineering Conference, Quito, Ecuador, 18-20 Nov., SPE 177060.

Nanson, G. C., & Page, K. (1983). Lateral accretion of fine-grained concave benches on meandering rivers. In: Collinson, J. D., & Lewin, J. (eds.) Modern and ancient fluvial systems, IAS Special Publication 6, 133-144.

Nardin, T. R., Feldman, H. R., & Carter, B. J. (2013). Stratigraphic architecture of a large-scale point-bar complex in the McMurray Formation: Syncrude's Mildred Lake Mine, Alberta, Canada. In: Hein, F. J., Leckie, D., Larter, S., & Suter, J. R. (eds.) Heavy-oil and oil-sand petroleum systems in Alberta and beyond, AAPG Studies in Geology, 64, 273-311.

Novakovic, D., White, C. D., Corbeanu, R. M., Hammon Iii, W. S., Bhattacharya, J. P., & McMechan, G. A. (2002). Hydraulic effects of shales in fluvial-deltaic deposits: ground-penetrating radar, outcrop observations, geostatistics, and three-dimensional flow modeling for the Ferron Sandstone, Utah. Mathematical Geology, 34, 857-893.

Pakdeesirote, A., Ackagosol, S., Geena, S., Kitvarayut, N. Lewis, K., Tran, T., Wildman, N., Soodsai, A., & Viriyasittigun, P. (2016) Horizontal well injector/producer pair Platong Field, Pattani Basin, Thailand. AAPG Search & Discovery Article #20354.

Pardo-Igúzquiza, E., & Dowd, P. A. (2003). CONNEC3D: a computer program for connectivity analysis of 3D random set models. Computers & Geosciences, 29, 775-785.

Parquer, M. N., Collon, P., & Caumon, G. (2017). Reconstruction of channelized systems through a conditioned reverse migration method. Mathematical Geosciences, 49, 965-994.

Posamentier, H. W. (2001). Lowstand alluvial bypass systems: incised vs. unincised. AAPG Bulletin, 85, 1771-1793.

Pouderoux, H. F., Pedersen, P. K., & Coderre, A. B. (2015). Fluvial reservoirs stacked in thin deltaic successions of the Lower Cretaceous Grand Rapids Formation, east-central Alberta, Canada. Interpretation, 3, T207-T232.

Pranter, M. J., Ellison, A. I., Cole, R. D., & Patterson, P. E. (2007). Analysis and modeling of intermediate-scale reservoir heterogeneity based on a fluvial point-bar outcrop analog, Williams Fork Formation, Piceance Basin, Colorado. AAPG Bulletin, 91, 1025-1051.

Pyrcz, M. J., & Deutsch, C. V. (2014). Geostatistical reservoir modeling. Oxford University Press, Oxford, 433 pp.

Pyrcz, M. J., Sech, R. P., Covault, J. A., Willis, B. J., Sylvester, Z., & Sun, T. (2015). Stratigraphic rule-based reservoir modeling. Bulletin of Canadian Petroleum Geology, 63, 287-303.

Reijenstein, H. M., Posamentier, H. W., & Bhattacharya, J. P. (2011). Seismic geomorphology and high-resolution seismic stratigraphy of inner-shelf fluvial, estuarine, deltaic, and marine sequences, Gulf of Thailand. AAPG Bulletin, 95, 1959-1990.

Remy, N., Boucher, A., & Wu, J. (2009). Applied geostatistics with SGeMS: a user's guide. Cambridge University Press, Cambridge, 264 pp.

Ritzi, R. W. (2000). Behavior of indicator variograms and transition probabilities in relation to the variance in lengths of hydrofacies. Water Resources Research, 36, 3375-3381.

Rongier, G., Collon, P., & Renard, P. (2017). A geostatistical approach to the simulation of stacked channels. Marine and Petroleum Geology, 82, 318-335.

Ruiu, J., Caumon, G., & Viseur, S. (2016). Modeling channel forms and related sedimentary objects using a boundary representation based on non-uniform rational B-splines. Mathematical Geosciences, 48, 259-284.

Shu, X., Hu, Y., Jin, B., Dong, R., Zhou, H., & Wang, J. (2015). Modeling Method of Point Bar Internal Architecture of Meandering River Reservoir Based on Meander Migration Process Inversion Algorithm and Virtual Geo-surfaces Automatic Fitting Technology. Society of Petroleum Engineers Annual Technical Conference and Exhibition, Houston, Texas, USA, 28-30 Sep., SPE 175013.

Smith, D. G., Hubbard, S. M., Lavigne, J. R., Leckie, D. A., & Fustic, M. (2011). Stratigraphy of counter-point-bar and eddy-accretion deposits in low-energy meander belts of the Peace-Athabasca Delta, northeast Alberta, Canada. In: Davidson, S. K., Leleu, S. & North, C. P. (eds.) From river to rock record: the preservation of fluvial sediments and their subsequent interpretation, SEPM Special Publication 97, 143-152.

Sonnenberg, S. A., McKenna, D. J., & McKenna, P. J. (1990). Sorrento field, Denver basin, Colorado. In: Sonnenberg, S. A., Shannon, L. T., Rader, K., von Drehle, W. F., & Martin, G. W. (eds.) Morrow sandstones of southeast Colorado and adjacent areas, Rocky Mountain Association of Geologists, Denver, 79-90.

Strebelle, S. (2002). Conditional simulation of complex geological structures using multiple-point statistics. Mathematical Geology, 34, 1-21.

Svanes, T., Martinius, A. W., Hegre, J., Maret, J. P., Mjs, R., & Molina, J. C. U. (2004). Integration of subsurface applications to develop a dynamic stochastic modeling workflow. AAPG Bulletin, 88, 1369-1390.

Thenin, D., & Larson, R. (2013). Quantitative seismic interpretation—An earth modeling perspective. CSEG Recorder, 38, 30-35.

Thomas, R. G., Smith, D. G., Wood, J. M., Visser, J., Calverley-Range, E. A., & Koster, E. H. (1987). Inclined heterolithic stratification—terminology, description, interpretation and significance. Sedimentary Geology, 53, 123-179.

van de Lageweg, W. I., van Dijk, W. M., Baar, A. W., Rutten, J., & Kleinhans, M. G. (2014). Bank pull or bar push: What drives scroll-bar formation in meandering rivers? Geology, 42, 319-322.

Wang, K., Wang, H., Shu, X., Zhou, D., Wang, R., Li, Y., Liu, N., Su, Z., & Ren, B. (2016). Super-large scale horizontal well position optimization method and infilling practice in high water-cut large complex fluvial reservoir based on multidisciplinary innovative techniques. Society of Petroleum Engineers Annual Technical Conference and Exhibition, Dubai, 26-28 Sep., SPE 181889.

Werren, E. G., Shew, R. D., Adams, E. R., & Stancliffe, R. J. (1990). Meander-belt reservoir geology, mid-dip Tuscaloosa, Little Creek field, Mississippi. In: Barwis, J. H., McPherson, J. G., & Studlick, J. R. (eds.) Sandstone petroleum reservoirs, Springer, New York, 85-107.

White, C. D. (2004). Geostatistical and flow modeling of intrareservoir mudstones. In: Scott, E. D., & Bouma, A. H. (eds.) Depositional processes and reservoir characteristics of siltstones, mudstones and shales, SEPM Miscellaneous Publication, 206-223.

Wightman, D. M., & Pemberton, S. G. (1997). The Lower Cretaceous (Aptian) McMurray Formation: an overview of the Fort McMurray area, northeastern, Alberta. In: Pemberton, S. G., & James, D. P. (eds.) Petroleum geology of the Cretaceous Mannville Group, western Canada, Canadian Society of Petroleum Geologists Memoir 18, 312-344.

Willis, B. J., & Tang, H. (2010). Three-dimensional connectivity of point-bar deposits. Journal of Sedimentary Research, 80, 440-454.

Wood, J. M. (1989). Alluvial architecture of the Upper Cretaceous Judith River Formation, Dinosaur Provincial Park, Alberta, Canada. Bulletin of Canadian Petroleum Geology, 37, 169-181.

Wu, S., Yue, D., Liu, J., Shu, Q., Fan, Z., & Li, Y. (2008). Hierarchy modeling of subsurface palaeochannel reservoir architecture. Science in China Series D: Earth Sciences, 51, 126-137.

Yan, N., Mountney, N. P., Colombera, L., & Dorrell, R. M. (2017). A 3D forward stratigraphic model of fluvial meander-bend evolution for prediction of point-bar lithofacies architecture. Computers & Geosciences, 105, 65-80.

Yan, N., Colombera, L., Mountney, N. P., & Dorrell R. (in press) Fluvial point-bar architecture and facies heterogeneity, and their influence on intra-bar static connectivity in humid coastal-plain and dryland fan systems. In: Ghinassi, M., Mountney, N. P., Colombera, L., & Reesink, A. J. (eds.) Meandering rivers and their depositional record, Special Publications of the International Association of Sedimentologists, 48, International Association of Sedimentologists.

Yin, Y. (2013). A new stochastic modeling of 3-D mud drapes inside point bar sands in meandering river deposits. Natural Resources Research, 22, 311-320.